
ONE AND TWO-PARTICLE SYSTEMS IN TOROIDAL
QUANTUM NANORINGS UNDER ADIABATIC
APPROXIMATION

MARLON RINCÓN FULLA



UNIVERSIDAD NACIONAL DE COLOMBIA
SEDE MEDELLÍN
FACULTAD DE CIENCIAS
ESCUELA DE FÍSICA
2010

ONE AND TWO-PARTICLE SYSTEMS IN TOROIDAL
QUANTUM NANORINGS UNDER ADIABATIC
APPROXIMATION

TRABAJO DE GRADO PARA OPTAR AL TÍTULO DE MÁGISTER EN CIENCIAS-FÍSICA

MARLON RINCÓN FULLA

DIRECTOR:

Ph.D JAIRO HUMBERTO MARÍN CADAVID



UNIVERSIDAD NACIONAL DE COLOMBIA
SEDE MEDELLÍN
FACULTAD DE CIENCIAS
ESCUELA DE FÍSICA
2010

NOTAS DE ACEPTACIÓN

Este trabajo fue revisado y avalado por:

Primer Jurado:

DR. LUIS ALBERTO SÁNCHEZ DUQUE
Escuela de Física
Universidad Nacional Sede Medellín

Fecha _____ Jurado _____

Segundo Jurado:

DR. AUGUSTO LEÓN MONTES BARAHONA
Instituto de Física
Universidad de Antioquia

Fecha _____ Jurado _____

Dedico este trabajo especialmente a mi madre Lucila Fulla, un ejemplo de resistencia, persistencia, lucha e irracional amor por lo que se ama... Un espíritu de ingenuidad con un inmenso universo de sabiduría... a María Girelsa quien accidentalmente abrió mis ojos a este infinito horizonte de conocimiento... y a todos aquellos quienes son compañía en esta caótica e impredecible existencia... M.F

Agradecimientos

Quiero expresar mis agradecimientos a la escuela de Física y a la Universidad Nacional, quienes financiaron la asistencia a los diferentes eventos nacionales e internacionales donde se presentaron las diferentes ponencias que hacen parte de este trabajo.

A mi madre María Lucila y mi hermana Julia Edith, por su incondicional apoyo y su diaria y cálida compañía.

Agradecimientos muy especiales al profesor Jairo Marín quien además de aceptar amablemente ser tutor de este trabajo, me invitó a contemplar un nuevo y cautivante mundo de conocimiento. A mis amigos y compañeros de maestría Diego Ortiz, Juan Manuel González, Sally Valbuena y Juan Luis Palacio, quienes me brindaron su camaradería en este sin límite y árduo camino de la búsqueda de respuestas para mi mente.

A Maria Girlesa, Felipe Arias y José Alvarez por preservar esa vieja amistad y por seguir compartiendo la misma pasión por la física y la ciencia.

A Juan Carlos Piña y todos los demás compañeros del grupo FICOMACO quienes hicieron aportes significativos y de forma paralela a mi trabajo.

Muy especialmente a mi amiga Carolina Sánchez por abrirme las puertas de su hogar y brindarme toda su hospitalidad en Ciudad de México, al igual que a todos los nuevos amigos del CINVESTAV.

Sean todos ustedes siempre muy bendecidos, infinitas gracias.

Nomenclature

TVS : Two vertically stacked
LDS : Low-dimensional system
SL : Super-lattice
QW : Quantum well
QWW: Quantum well wire
QD : Quantum dot
SAQD: Self-assembled quantum dot
QR : Quantum ring
AFM : Atomic force microscopy
TQR : Toroidal quantum ring
CS : Cross-section
VSN : Vertically stacked nanorings
TES : Two-electron system

Abstract

In this work is presented a theoretical study of several two-particle systems, such as the case of an electron-electron and a electron-hole system (assuming the same effective mass for both particles) constrained to move into semiconductor quantum rings in a hard-wall confinement regime. The study of these charge carriers into these nanostructures was done within the effective mass approximation. The framework was pointed out to the calculation and interpretation of the system energy spectrum.

In general, since the model Hamiltonians related to these systems are not exactly solvable, it was necessary to implement the adiabatic approximation whose application is only valid when the quantum rings are very narrow. This fact has been verified experimentally for the case of self-assembled quantum rings by means of atomic force microscopy techniques. In this sense, this method is reasonable and adequate for describing in first approximation real quantum ring-shaped systems. Physically, the using of adiabatic approximation, allows to decouple the fast particles' motion along the cross section of the rings from their slow orbital motion around the system symmetry axis.

With the aim of establishing the size and shape effects on the energy spectrum, it was studied the two-particle problem in two vertically stacked one-dimensional quantum rings, in two concentric quantum ribbons, in two-dimensional flat rings (washer-shaped) and in two vertically stacked toroidal quantum rings with three different cross-sections morphologies (square, rectangular and circular). Furthermore, it was studied these systems in presence of impurities donors, where it was shown that the energy spectrum of such nanostructures is very similar to the energy spectrum of an actual molecule, by this reason they are often called artificial molecules. Finally motivated by a great amount of theoretical and experimental works, it was considered these systems under the presence of an uniform static axial magnetic field which give rise to an interesting oscillatory phenomenon of the spin-shift of the system's ground state known as the Aharonov-Bohm effect.

Part of the computational modeling related to the analyzed systems in the present work, was done within the project funded by DIME: "*Efecto de la morfología sobre el espectro energético de una y dos partículas en anillos cuánticos acoplados*". Bicentenario 2008-2009. Cod. QUIPU 20101007748.

The results obtained in this work were presented and socialized in the following events:

- VIII ESCUELA NACIONAL DE FÍSICA DE LA MATERIA CONDENSADA (VIII ENFMC), Pereira-Colombia (2008)
- 32nd INTERNATIONAL SYMPOSIUM ON DYNAMICAL PROPERTIES OF SOLIDS, Antwerp-Belgium (2009)
- XXIII CONGRESO NACIONAL DE FISICA Santa Marta-Colombia (2009)
- PHYSICS OF LIGHT-MATTER COUPLING IN NANOSTRUCTURES 2010 (PLMCN10) Cuernavaca-Mexico (2010)
- IX ESCUELA NACIONAL DE FÍSICA DE LA MATERIA CONDENSADA (IX ENFMC), Ibagué-Colombia (2019)

Additionally, the study of the systems mentioned above has led to the realization of the following accepted works to be published in the **Superlattices and Microstructures** Journal:

- *Spectral properties of two electrons vertically coupled in toroidal quantum rings (Article in Press, Corrected Proof doi:10.1016/j.spmi.2010.07.002)*
- *Energy spectrum of an artificial molecular complex in toroidal quantum rings (Article in Press, Corrected Proof doi:10.1016/j.spmi.2010.07.004)*

Some of the results were summarized and submitted in the works (currently in proof process) entitled:

- *Electron-electron correlation in vertically stacked nanorings (**Revista Colombiana de Física**)*

- *Two-electron energy spectrum in concentrically coupled quantum ribbons (**Revista Colombiana de Física**)*
- *Energy structure of two electrons in torous-shaped quantum ring (**Revista Tumbaga**)*
- *Aharonov-Bohm effect in two concentrically toroidal quantum rings (**Revista Tumbaga**)*
- *Transition from an artificial Hydrogen molecule to a negative hydrogen Ion D^- (**Revista Tumbaga**)*

Resumen

En este trabajo se presenta un estudio teórico de varios sistemas bi-particulares, como es el caso de un sistema electrón-electrón y electrón-hueco (asumiendo masas efectivas iguales para ambas partículas) restringidos a moverse en anillos cuánticos semiconductores dentro de un régimen de confinamiento infinito. El estudio de estos sistemas nano-estructurados fue hecho bajo la aproximación de masa efectiva y se centró en el cálculo e interpretación del espectro energético del sistema.

Dado que el Hamiltoniano que describe estos sistemas en general no presenta soluciones exactas, se implementó el método de la aproximación adiabática, el cual es válido si se garantiza que los anillos cuánticos a analizar son muy delgados. Éste hecho se ha sido visualizado experimentalmente para el caso de los anillos cuánticos autoensamblados mediante técnicas de microscopía de fuerza atómica. Así, en este sentido, éste método es adecuado y razonable para llevar a cabo una descripción (en una primera aproximación) de las propiedades energéticas de sistemas reales de anillos cuánticos. Físicamente, la implementación de la aproximación adiabática, permite desacoplar el movimiento rápido de las partículas a lo largo de la sección transversal de los anillos, del movimiento orbital lento alrededor del eje de simetría del sistema.

Con el ánimo de establecer los efectos de tamaño y forma sobre el espectro energético, se estudió sistemas de dos partículas en anillos unidimensionales acoplados verticalmente, en dos cintas cuánticas concéntricas, en anillos planos (con forma de arandela) y en dos anillos cuánticos toroidales acoplados verticalmente con tres diferentes morfologías de sección transversal (cuadrada, rectangular y circular). Adicionalmente, se estudió estos sistemas en presencia de impurezas donadoras, donde se muestra que el espectro energético de estas configuraciones presenta similitudes con el espectro energético de una molécula natural, y por esta razón son a menudo llamadas moléculas artificiales. Finalmente dada la motivación generada por la gran cantidad de trabajos tanto teóricos como experimentales, se considera estos sistemas en presencia de un campo magnético uniforme, estático y axial el cuál da origen a un interesante fenómeno oscilatorio del cambio del spin asociado al estado base del sistema conocido como el efecto Aharonov-Bohm.

Parte de los cálculos computacionales relacionados con los sistemas analizados en este trabajo, se realizaron dentro del marco del proyecto financiado por el DIME: "*Efecto de la morfología sobre el espectro energético de una y dos partículas en anillos cuánticos acoplados*". Bicentenario 2008-2009. Cod. QUIPU 20101007748.

Los resultados obtenidos en este trabajo se presentaron y socializaron en los siguientes eventos:

- VIII ESCUELA NACIONAL DE FÍSICA DE LA MATERIA CONDENSADA (VIII ENFMC), Pereira-Colombia (2008)
- 32nd INTERNATIONAL SYMPOSIUM ON DYNAMICAL PROPERTIES OF SOLIDS, Antwerp-Bélgica (2009)
- XXIII CONGRESO NACIONAL DE FISICA Santa Marta-Colombia (2009)
- PHYSICS OF LIGHT-MATTER COUPLING IN NANOSTRUCTURES 2010 (PLMCN10) Cuernavaca-Mexico (2010)
- IX ESCUELA NACIONAL DE FÍSICA DE LA MATERIA CONDENSADA (IX ENFMC), Ibagué-Colombia (2019)

Adicionalmente, el estudio de los sistemas mencionados arriba, dieron origen a la realización de los siguientes trabajos aceptados para ser publicados en la revista **Superlattices and Microstructures** :

- *Spectral properties of two electrons vertically coupled in toroidal quantum rings (Article in Press, Corrected Proof doi:10.1016/j.spmi.2010.07.002)*
- *Energy spectrum of an artificial molecular complex in toroidal quantum rings(Article in Press, Corrected Proof doi:10.1016/j.spmi.2010.07.004)*

Algunos de los resultados fueron sintetizados y sometidos a evaluación en los trabajos titulados (actualmente en proceso de evaluación):

- *Electron-electron correlation in vertically stacked nanorings (Revista Colombiana de Física)*

- *Two-electron energy spectrum in concentrically coupled quantum ribbons (**Revista Colombiana de Física**)*
- *Energy structure of two electrons in torus-shaped quantum ring (**Revista Tumbaga**)*
- *Aharonov-Bohm effect in two concentrically toroidal quantum rings (**Revista Tumbaga**)*
- *Transition from an artificial Hydrogen molecule to a negative hydrogen Ion D^- (**Revista Tumbaga**)*

Contents

Nomenclature	vi
Abstract	vii
List of Figures	xvi
1 Introduction	1
2 Model and Computational Tools	8
2.1 The System Hamiltonian	9
2.1.1 Dimensionless Hamiltonian	10
2.1.2 Ring-System Geometries	11
2.2 Adiabatic Approximation	14
2.2.1 Centre-of-Mass and Relative Coordinates	15
2.2.2 Model Validation	16
2.2.3 Solution algorithm using adiabatic approximation	19
2.2.4 Quantum rings and donor impurities	20
2.3 Numerical methods and computational tools	21
3 One-dimensional quasi-exactly solvable systems	22
3.1 System Hamiltonian	23
3.2 Wigner Crystallization in one-dimensional vertically coupled rings	25
3.3 Aharonov-Bohm effect in one-dimensional vertically coupled rings	26
3.4 Size effect on the one-dimensional vertically coupled rings spectrum	28
4 Two-dimensional systems	30
4.1 Two-particle systems in Nanoribbons	30
4.1.1 System Hamiltonian	31
4.1.2 Size effects and the influence of the magnetic field	34
4.1.3 Electron-hole pair with same effective masses and Wigner crystallization	35
4.2 One and two-particle systems in flat ring-shaped quantum dots	36
4.2.1 System Hamiltonian	37

<i>CONTENTS</i>	xiv
4.2.2 Size effects on the energy spectrum	38
4.2.3 Aharonov-Bohm effect in two-dimensional systems	39
5 Toroidal quantum rings	41
5.1 System Hamiltonian	41
5.2 Two-electron eigenfunctions and probability densities	43
5.3 Electron-electron correlation and its influence on the Wigner Crystallization	45
5.4 Aharonov-Bohm effect in vertically coupled toroidal quantum rings	47
6 Artificial Molecules	49
6.1 System Hamiltonian	49
6.2 Size and impurities location effects on the molecular energy spectrum	52
6.3 Artificial molecule in presence of an uniform magnetic field	55
Conclusions	57
A Trigonometric Sweep Method	59
B Simplified notation for Low-lying states	63
References	69

List of Figures

1.1	Quantum ring micrographs	4
1.2	Vertically coupled and concentric quantum rings micrographs	5
2.1	TQRs System geometries	12
2.2	Redefinition of the particle vector position and the $X_{t_k} - Z_{t_k}$ plane	13
2.3	Transformation of the $X_{t_k} - Z_{t_k}$ to the $\bar{X}_{t_k} - \bar{Z}_{t_k}$ plane	18
3.1	One-dimensional vertically coupled nanorings and some low-lying renormalized energies in the limiting case as the interrings distance tends to zero	24
3.2	Wigner Crystallization in one-dimensional vertically coupled rings	25
3.3	Renormalized energy as a function of γ parameter for TVS nanorings for several values of α parameter	27
3.4	Three dimensional curve of the renormalized energy as a function of α and β parameters	28
3.5	Renormalized energy as a function of the radii ratio	29
4.1	Two-particle system into two concentric nanoribbons and some low-lying energies as a function of the ribbon's inner radius and different values of α parameter and ribbon's height	32
4.2	Renormalized energy as a function of α in presence of magnetic field	35
4.3	Total renormalized energy of an electron-hole system as function of the inner radius	36
4.4	Schematic 3D-diagram of a flat ring confining two electrons in presence of two donor impurities	37
4.5	Total renormalized energy as function of the center-line radius for a one and two-particle system in flat rings with two-on axis impurities	38
4.6	Total renormalized energy as function of the magnetic field strength for a one and two-particle system in a flat ring, and a two-particle system in two concentric nanoribbons	40

5.1	Schematic 3D diagram of two electrons in vertically coupled TQRs with rectangular, circular and square cross-sections	42
5.2	Two-electron probability densities	44
5.3	Energies $\tilde{E}(M, m, s)$ as a function of the centre-line radius for two different shapes of the torus cross-sections: circular and square	46
5.4	Evolution of the energies of the first low-lying states as a function of the centre-line radius for tori with square cross-section by varying d and α parameters .	47
5.5	Energies $\tilde{E}(M, m, s)$ as a function of the renormalized magnetic field strength for tori with circular, square and rectangular CSs	48
6.1	Three-dimensional model image of an artificial hydrogen molecule	50
6.2	Ground-state energy of an artificial hydrogen molecule as a function of the distance between ions for different ring thicknesses and ring radii	53
6.3	Some of the low-lying energy levels of an artificial hydrogen molecule as a function of the distance between ions.	54
6.4	The lowest energy levels of an artificial hydrogen molecule as a function of the renormalized magnetic field	55
A.1	Phase-space plane of Poincaré polar coordinates	60

List of Tables

4.1	Comparison between exact energy values corresponding to [26] and the energy values obtained for two electrons in two concentric quantum ribbons for a set of three different values of α and h parameters	34
5.1	Comparison between the two-electron energies $\tilde{E}(M, m, s)$ obtained in this work for the limiting case ($R_t \rightarrow 0, \alpha \rightarrow 1$) with those previously reported in [26, 27]	43
6.1	Some of the renormalized low-lying energy levels $\tilde{E} = R^2 E(M, m, s)$ of the artificial hydrogen molecule for two different radii of the centre-line R and four different separations ζ between ions	52
B.1	Energy labeling notation for some low-lying states for the two-electron system	63

Chapter 1

Introduction

The recent advances obtained by low-scale physics in the materials science have led to the development of exotic and extraordinary applications, revolutionizing radically the role of technology in contemporary world. The medical sciences, the telecommunications, the sensors and optoelectronic industry have been the more benefited fields. These advances have motivated to realize enterprising high technological projects as the processors of quantum information [1], among other applications that a few years ago would have been inconceivable such is the case of the astonishing quantum teleportation systems [2]. These are some of the promising developments to be achieved by one of the most innovative and modern fields of the human knowledge, which has been defined as nanotechnology [3].

The invention of new devices has led to develop a high degree of sophistication and control over materials growth techniques, allowing the fabrication of diverse artificial structures with innovating properties and very different in contrast with those exhibited by bulk materials. This is the case of semiconductor heterostructures [4, 5, 6] whose size and morphology can be predetermined and adjusted with nanometric precision, by this reason they are called low-dimensional systems (LDS).

Pioneer studies on semiconductor nanostructures were done in the seventies by Esaki and Tsu [7], who researching for IBM, they could establish the first basis of the superlattices (SL) growth techniques [4, 5, 6]. These systems are fabricated by the periodic and alternating stacking up of two semiconductor materials A and B, such as GaAs and the GaAlAs, which are characterized by having dissimilar energy gaps and small lattice parameter mismatch. The heterojunction is formed by depositing thin films of the materials with nanometric thicknesses following an ABABA sequence. Initially these systems were grown by molecular beam epitaxy (MBE) [4, 5, 6], subsequently by using the chemical vapor deposition (CVD) [4, 5, 6].

In parallel with the SLs development, an innovative semiconductor structure was possible to grow and received the name of quantum well (QW) [5]. Which is defined basically as an heterojunction of two semiconductors A and B placed in the form ABA, where the inner semiconductor B has the smaller energy gap. An additional condition is that the semiconductor layers have thicknesses smaller than the de Broglie wavelength associated to the carriers confined in the structure. This morphological condition leads to reduce in one degree of freedom the particles motion, giving rise only to a two-dimensional motion on a plane which is perpendicular to the growth direction. This is the reason by which QWs are often called two-dimensional structures. Further on, at the end of eighties, the refinement achieved in the growth techniques, allowed to fabricate the called quantum well wires (QWWs) [5], where the particles motion was restricted in an additional degree of freedom, giving rise to the possibility of moving only in quasi-one-dimensional spaces. The restricting process on the particles motion ended with the fabrication of novel and promising nanostructures called quantum dots (QDs) [8], in which the carriers are restricted to move in zero-dimensional spaces.

Among the great variety of LDSs that are fabricated, those that have captured the attention of researchers and also creating high expectations in the scientific community, correspond to the QDs. This fact has motivated a great production of theoretical and experimental works published in the last years. From the nano-physics point of view, due to the strong confinement that particles undergo into these structures, the QDs constitute a low-scale laboratories in which is possible to realize a more rigorous and simplest study of the correlation effects between electron-electron, electron-hole, and donor-electron systems. Furthermore, it is possible to examine in detail the actual incidence of these interactions on the energy spectrum and on the transport properties. From a technological point of view, the QDs have allowed to achieve great advances in optoelectronics as a result of the electronic devices miniaturization, here may be mentioned the quantum dot lasers [1, 9, 10], photo-detectors [9, 11, 12], emitters [9, 13] and one-single transistors [14, 15].

Within the wide range of QDs fabricated nowadays, those that have been a great deal of attention are the denominated self-assembled quantum dots (SAQDs) which are obtained by a crystal growth process called the Stranki-Krastanow technique [9]. In this procedure the QDs grow spontaneously due to the simultaneous effects of temperature and stress-relaxation phenomena, that are presented when a semiconductor is deposited over a substrate with slightly different lattice parameter. This situation allows the formation of 3D-islands with diverse morphologies, here, it is worthwhile to mention the QDs lens-like, pyramidal, disk and ring-shaped. One of the most relevant structural properties of the SAQDs is that the

lateral size, which is usually between 30-70nm, it is much greater than the height which is about 2-4nm. This experimental fact has made that many authors consider two-dimensional models in order to obtain the structure of the energy spectrum of systems compound by one [16, 17] and two electrons [18, 19], excitons [20, 21], trions[22] and donor impurities[23, 24].

In spite of two-dimensional models reduce significantly the computing process to obtain the energy spectrum, it is necessary to notice that from a physical point of view these models make no sense at all, because it could not obtain discrete energy levels since the conditions for wavefunction overflowing would outweigh, giving rise to a continuous energy spectrum. Additionally, considering strictly two-dimensional models, the effects on the energy spectrum by the QD morphology and the confinement potential that is strongly dependent on the transversal profile, would be neglected. Within the wide variety of SAQDs recently fabricated, those ones that have been a great deal of attention are the called quantum rings (QRs), since these nanoscopic structures allow to extrapolate to one and two-dimensional systems by means of topological variations. The first QR obtained experimentally was achieved by Lorke and co-workers [1, 25] by using self-assembling techniques. The grown QRs were characterized by having inner and outer radii whose dimensions varied between 10-20nm and 30-70nm respectively, while the QRs height does not exceed the 2-6 nm. In Fig.1.1 can be appreciated a set of QRs which morphology has been analyzed by means of atomic force microscopy (AFM). Since the QR height is small, some authors have assumed the QRs as two-dimensional systems [16, 24]; even others have considered the simplest case, assuming the QRs as if they were strictly one-dimensional systems [26, 27].

The discovery of QRs have inspired the production of diverse theoretical studies [17, 19, 21, 23] being of great interest those related with magnetic field effects, because they allow to establish the existence of induced ground-state transitions. Recently, some researchers have reported the possibility of fabricating devices based on toroidal quantum rings (TQRs) of InGaAs [28, 29, 30], in which the simplest configurations to be analyzed are the few-particle systems, for instance, a single electron or an ionized donor impurity confined in a single TQR [31] or in a pair of concentric TQRs [32]. These systems have been study under the matrix diagonalization method [33] and the variational method in association with the adiabatic approximation [34]. The results show that the energy spectrum is strongly dependent on the QR size and the location of the impurities.

The few-particle systems are very important because they constitute fundamental models in physics, mainly in the atomic, molecular and solid state physics. In the last case, the study of few-particle systems related to semiconductor materials, it is a great focus of attention, since the electronic and optical properties that could be obtained with technological purposes

[1, 5, 8], are strongly dependent on the concentration and the type of particles within the material.

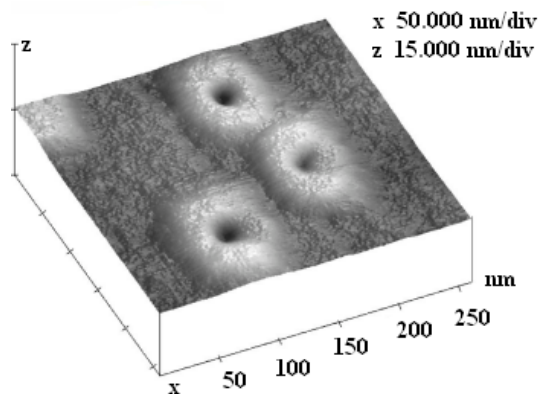


Figure 1.1: AFM micrograph of a collection of self-assembled QRs with typical heights ranging from the 2 to 6nm, and characterized by inner and outer radii of the order of 10nm to 20nm and 30 to 70 nm, respectively (image extracted from [35]).

A complete description of these systems, requires to include the interaction between particles making unviable to find exact solutions of the Schrödinger equation. For this reason is necessary to resort to approximate methods, including the variational method [36, 37, 38], the matrix diagonalization [33], Hartree-Fock [33, 39], density functional theory [39], Monte-Carlo method [40] among others. The theoretical study of few-particle systems also clarifies and explains in a simple way the actual incidence of the correlation effects on the energy spectrum and its influence over the electronic transport properties. The models devised in order to study the few-particle systems are very important because they reveal clearly some general and essential properties that also characterize the multi-particle systems. In the recent years, the interest by few-particle problems has been boosted significantly as consequence of the QDs fabrication. Basically this is due to the fact that they confine spatially the particles in the three directions, originating a rising in the systems' energy as a result of the substantial increment in the Coulomb interaction, which can be explained as a direct effect of the particles rapprochement. This fact has made possible to observe experimentally at room temperature, diverse few-particle systems [25, 41, 42], which is practically impossible of realizing in bulk semiconductors, since at temperatures over the $5^\circ K$ the thermal energy exceeds the ionization energy making that the systems become unstable.

The adiabatic approximation is another method which could be implemented to analyze few-particles systems in quantum dots, allowing to have into account the quantum ring morphology on the energy spectrum [34]. Several few-particle systems are possible to be analyzed with this method, for instance, two electrons or an electron-hole pair, when they are confined either in one-single ring, or when they are spatially separated in two vertically coupled rings [43] or in concentric rings [32, 41] (see Fig.1.2). These double-ring systems have been found experimentally [41, 43] and the theoretical study of their energy spectrum still being object of discussion and is leading to extensive researches [27, 32, 44, 45, 46]. The importance of these systems lies on the possibility of analyzing the influence of the correlation effects among particles under strong confinement conditions, because the QRs energy spectrum in a quantum regimen exhibit interesting properties that are strongly dependent on the composition, size, shape, interring-distances, as well as the nature of the external applied fields (magnetic and electric fields and hydrostatic pressure); situations that are not possible to see in bulk semiconductors.

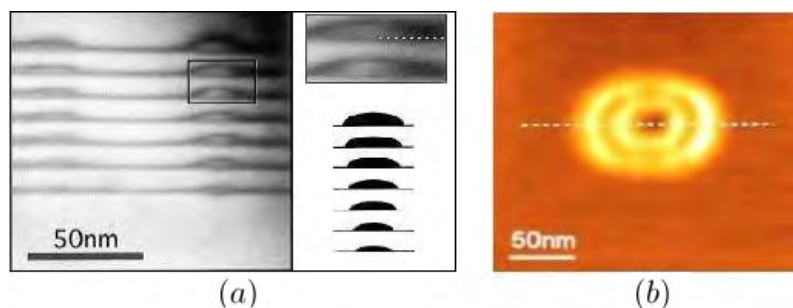


Figure 1.2: AFM Micrographs of QRs vertically coupled (image extracted from [41])(a) and placed concentrically (image extracted from [43])(b).

Motivated by the theoretical importance and the technological incidence of vertically coupled and concentric TQRs mentioned above, in the present work is proposed to study one and two-particle systems forced to move into single or in quantum double-ring configurations. In this sense, using an approximate method is necessary to solve the system Hamiltonian, and the adiabatic approximation is adequate since agrees with the experimental fact that claims the self-assembled QRs thicknesses are small in comparison with their lateral size.

In order to accomplish this purpose, a versatile model consisting of two vertically coupled narrow TQRs with different radii is considered, which is able to extrapolate the concentric rings situation by reducing the interring distance to zero. It is important to point out that

TQRs thicknesses will be assumed very small but not negligible. Furthermore, with the aim of establishing the incidence of external fields on the energy spectrum, the system is considered in presence of an homogeneous static magnetic field applied along the symmetry axis. In this sense, the developed models in the present work are intrinsically more general than those analyzed in the references.

Despite of considering narrow TQRs, it is desired to explore the incidence that the cross-section (CS) morphology has on the energy spectrum, since the electron-electron interaction, the shape and size of the QRs still being an interesting subject of researching. An additional topic of interest in this work, is the analysis and determination of the geometrical conditions of separation between rings in which the formation of Wigner-type crystals are given, in this particular case, with only two particles.

With the aim of realizing a complete and detailed study of the geometry influence on the energy spectrum, in chapters 3 and 4, it is analyzed one and two-dimensional systems, respectively. The results obtained allows to describe the evolution of the spectral properties as is considered progressively an additional dimension, starting from strictly one-dimensional rings, then considering a flat-ring and ribbon morphologies and finally TQRs systems. Moreover, taking advantage of the fact that the two-particle problem in one-dimensional QRs systems is quasi-exactly solvable [26, 27] and the two-dimensional ones describe in a simplest way the behavior of the confined system, their study will provide results to support and validate those obtained for TQRs in limiting cases. For instance, the TQRs system energy spectrum must consistently tend to the energy spectrum of strict one-dimensional ring system as the CS dimensions tend to zero (certainly, maintaining fixed the geometry, the characteristics of the field, the number and the nature of the confined particles).

In chapter 5, the TQRs systems are analyzed, where the CS ring morphology were considered with the purpose of modeling more realistic situations. It is presented in detail the spectral properties in connection with the size and shape effects and the influence of the magnetic field. For this purpose, it will be considered three different shapes of TQRs cross-sections, circular, square and rectangular. The advantage of considering these morphologies is that by a carefully adjusting of the geometrical parameters, the strict cases one and two-dimensional can be obtained as limiting cases of the proposed model, allowing to establish the quality of the results since for two-electron systems in one-dimensional rings, Zhu and coworkers have obtained exact solutions [26].

Finally, In chapter 6 it is considered TQRs in presence of on-axis donor impurities, giving rise to a more complex energy spectrum as a result of additional interactions between the

negative charge carriers confined inside the rings and the surrounding impurities. It will be shown that the energy spectrum as a function of the inter-donor separation has a similar behavior to spectrum of molecules provided by the nature. Thus, in this sense, an astonishing and very promising application of these low sized systems is the fabrication of artificial molecules whose characteristic energy spectrum can be manipulated and tailored by varying geometrical parameters such as the interring distance, the ring centre-lines ratio or the CS morphology.

As can be noticed at this point, tailoring energy spectra of nanostructures is still open to new ideas and aimed by the possibility of implementing such systems in outstanding technological applications to be developed in the near future.

In the following chapter (2) it will be presented the model proposed in the study of TQRs, enclosed with some definitions of geometrical parameters and a brief explanation of the adiabatic approximation method in physics. In a more focused way, it will be analyzed the validity of this method aimed toward TQRs and the methodology to follow in the solution of the system Hamiltonian. Subsequently, it is presented the numerical solution algorithm of the eigenvalue problem determined by the Hamiltonian in the adiabatic regime, which it is applied to the studied systems in chapters 4, 5 and 6. Finally, it is briefly mentioned some important computational tools to be used in the analyzed systems throughout the document.

Chapter 2

Model and Computational Tools

In the present work, it will be modeled N-particle systems confined in self-assembled semiconductors QRs. The N-index is related to the number of particles being considered, taking the values of 1 and 2 for the cases of one and two-particle systems in that order. The ring-shaped confinement potential is formed as a consequence of the energy gap difference between the two component materials which the quantum dot is made of [8], and will be considered equal to zero and infinite inside and outside of the QRs, respectively.

It will be shown thorough the subsequent chapters that the vertically coupled QRs model with different radii is a general case, that allows to study other systems as limiting cases, when a cautious adjusting of geometrical parameters such as the ring radii ratio or the inter-ring distance is done. For instance, the two-particle system confined in one single ring, is expected to be obtained as a limiting case as the inter-ring distance tends to zero between two vertically coupled QRs with same radii and confining one particle separately .

It is worthwhile to mention when only one single particle is studied, we shall have basically a one-particle system constrained to move only into a single QR, since the potential confinement is infinite outside the torous and it would hamper the particle to tunnel to the other ring.

This versatile model allows to show the strong dependence of the energy spectrum on the geometry in which the rings are set, and also explains the interplay between some geometrical parameters and the behavior of other phenomena such the Aharonov-Bohm effect [37], which is a clear evidence of the vector potential influence on these kinds of heterostructures. This amazing phenomenon in the semiconductor QRs becomes apparent as the oscillatory and periodic spin-shift related to the ground state, giving rise to transitions in the sequence

singlet-triplet-singlet when the magnetic field strength is increased.

On the computational side, one of the advantages offered by versatile models in physics, is to facilitate some development tasks, such as writing encapsulated source code, performing efficiently debugging processes and detecting errors and exceptions. In this sense, to be successful in numerical modeling of physical systems, it is fundamental to find the more convenient and proper way to represent the system in the build source code [47].

In the next section it will be presented the system Hamiltonian of two particles confined in two vertically coupled TQRs which are placed in two parallel planes. This Hamiltonian written in such general form will allow to study the size and shape effects on the energy spectrum and the Aharonov-Bohm oscillations. Additionally, given the versatility of the model, it will be analyzed other systems of reduced dimension such as one-dimensional rings, flat rings (washer-shaped) and nanoribbons.

2.1 The System Hamiltonian

As mentioned above, the most general system considers two particles constrained to move separately inside of two coaxial and vertically stacked nanorings whose contours define an infinite well ring-shaped confinement potential represented by $\hat{U}_k(\vec{r}_k)$, where the k -index denotes each particle ($k = 1, 2$) and \vec{r}_k are the respective vector positions.

When two particles are considered, the Coulomb particle-particle interaction is included in the Hamiltonian and will be denoted by $\hat{V}(|\vec{r}_2 - \vec{r}_1|)$. This repulsion/attraction energy is a quantity that depends on the relative distance between particles $|\vec{r}_2 - \vec{r}_1|$, the media and the charges of the particles under consideration. In chapter 6, TQRs systems in presence of on-axis donor impurities will be subject of study, thus additional terms related to Coulomb interactions will be included later.

Other interesting developments involve the applying of external fields, this fact motivates to consider the presence of an homogeneous static magnetic field $\vec{B} = B\hat{k}$ threading the interior of the rings and oriented along the common symmetry axis.

Consequently, having these elements in mind, the system Hamiltonian (for one and two-particle systems) under the effective mass approximation can be written as:

$$\hat{H} = \sum_{k=1}^N \left[\frac{(\hat{\vec{P}}_k + \frac{e}{c} \tau_k \hat{\vec{A}}_k)^2}{2m^*} + \hat{U}_k(\vec{r}_k) \right] + \hat{V}(|\vec{r}_2 - \vec{r}_1|) \quad (2.1a)$$

$$\hat{\vec{A}}_k = -\frac{1}{2} \hat{\vec{r}}_k \times \vec{B} \quad (2.1b)$$

Here, it is considered the same effective mass m^* for both particles and it is assumed that the vector potential satisfies the Coulomb gauge condition (2.1b), in order to obtain the magnetic field described above. On the other hand, τ_k is a parameter introduced as the unitary charge, equal to 1 and -1 for holes and electrons respectively.

The rotational motion of the particles around the symmetry axis suggests that the more adequate coordinate system to study the problem corresponds to the cylindrical coordinates (ρ_k, φ_k, z_k) . The system Hamiltonian (2.1) written explicitly in this coordinate system takes the form:

$$\hat{H} = \sum_{k=1}^N \left[-\frac{\hbar^2}{2m^*} \nabla_k^2 - \frac{i\hbar e \tau_k B}{2m^* c} \frac{\partial}{\partial \varphi_k} + \frac{e^2 B^2}{8m^* c^2} \rho_k^2 + \hat{U}_k(\vec{r}_k) \right] + \hat{V}(|\vec{r}_2 - \vec{r}_1|) \quad (2.2)$$

Where the terms appearing in (2.2) are related to the kinetic energy operator, the paramagnetic and diamagnetic terms due to the presence of the magnetic field (terms proportional to the first and second power of the magnetic field strength respectively), the confinement potential and finally the Coulomb interaction, in that order from left to right.

2.1.1 Dimensionless Hamiltonian

Dealing with small quantities such \hbar^2 in computational processes, usually leads to errors because of overflowing, even if variables of maximum precision are used (double precision data). In some programming environments simply is not possible to define any kind of variable able to store such quantities. For this reason is necessary to redefine the Hamiltonian in terms of effective units, which will allow us to rescale the physical quantities and transform them into other ones computationally runnable, for example in Fortran environments [47]. For this purpose are introduced the effective Bohr radius $a_0^* = \hbar^2 \epsilon / m^* e^2$, the effective Rydberg $Ry^* = e^2 / 2\epsilon a_0^*$ and $\gamma = e\hbar B / 2m^* c Ry^*$, that will be taken as units of length, energy and the conventional dimensionless magnetic field strength, respectively.

The dimensionless coordinates and energy, will be labeled with an upper bar symbol and are defined by the expressions (2.3a) and (2.3b) as follows:

$$\rho_k = \bar{\rho}_k a_0^* \quad ; \quad z_k = \bar{z}_k a_0^* \quad (2.3a)$$

$$E = \bar{E} R_y^* \quad (2.3b)$$

Taking into account the effective units and definitions (2.3), is easy to show that Hamiltonian (2.2) can be rewritten as the following system dimensionless Hamiltonian:

$$\hat{H} = \sum_{k=1}^N \left[-\bar{\nabla}_k^2 - i\tau_k \gamma \frac{\partial}{\partial \varphi_k} + \frac{\gamma^2}{4} \bar{\rho}_k^2 + \hat{U}_k(\vec{r}_k) \right] + \hat{V}(|\vec{r}_2 - \vec{r}_1|) = \bar{E} \quad (2.4a)$$

$$\hat{V}(|\vec{r}_2 - \vec{r}_1|) = \frac{2\tau_1 \tau_2}{|\vec{r}_2 - \vec{r}_1|} \quad (2.4b)$$

Here, $\hat{V}(|\vec{r}_2 - \vec{r}_1|) = \hat{V}(|r_2^z - r_1^z|) R_y^*$ is the dimensionless Coulomb particle-particle interaction, τ_1 and τ_2 are the particles unitary charges, and \vec{r}_1 and \vec{r}_2 their dimensionless vector positions.

Given the computational advantages of effective units, from this point and throughout the document unless otherwise is stated, the quantities will be assumed dimensionless and the upper bar symbol will be omitted by simplicity.

2.1.2 Ring-System Geometries

An important aspect to bear in mind is the relative geometrical disposition of the rings and their morphological characteristics. With the aim of studying the influence on the energy spectrum by the CS geometry, in this work will be consider three different CS morphologies (circular, rectangular and square). For comparison purposes the square and circular CS were taken with same area and equal to πR_t^2 , where the circular CS has a radius R_t and the square one has side $h = \sqrt{\pi} R_t$. In order to analyze asymmetric situations the rectangular CS has been taken with height l and adjustable width w (see Fig. 2.1(a)).

For each ring individually, it is introduced the centre-line, defined as a circumference with origin located on the symmetry axis and passing thorough the CS centroid. The centre-lines have radii $R_1 = R$ and $R_2 = \alpha R$ for lower and upper ring respectively. The inter-ring distance will be denoted by $d = \beta R$ and its value coincides with the distance between the parallel planes which contains the centre-lines (see Fig. 2.1(b)). The R parameter will be defined as the half the sum of the outer (R_{out}) and inner (R_{in}) ring radii (see Fig. 2.1(c)), α

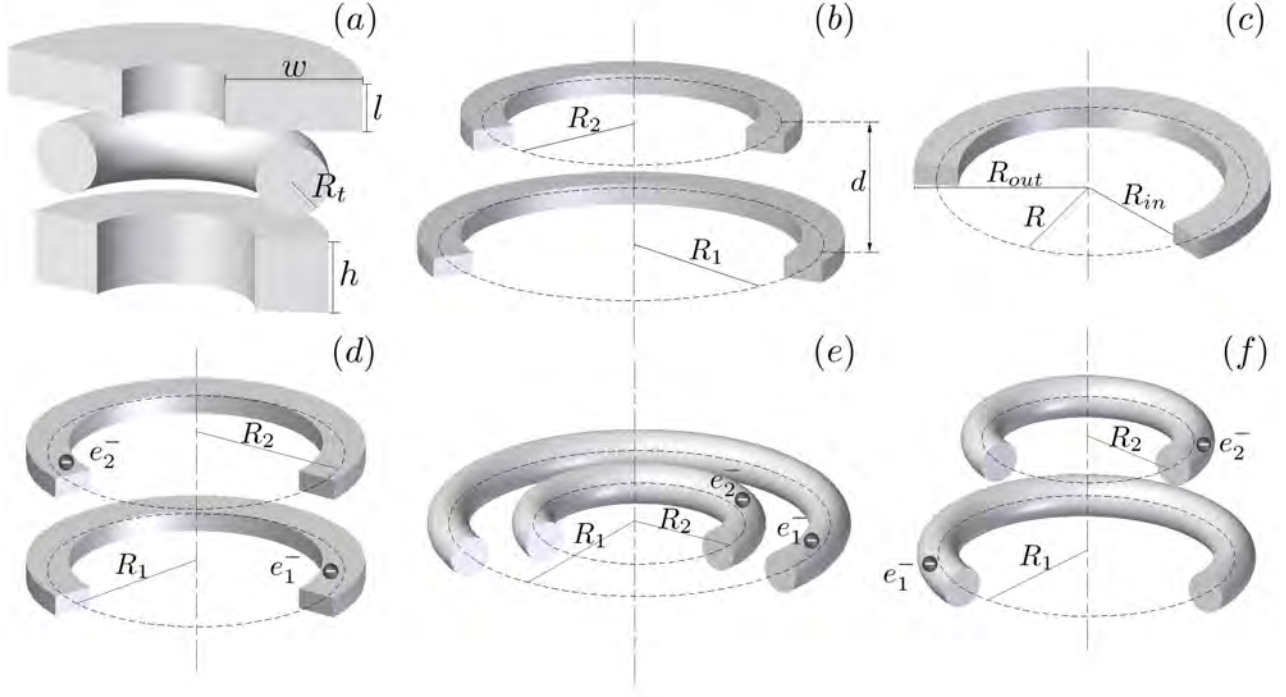


Figure 2.1: Three different CS geometries (a). The most general case considers two rings vertically coupled with different radii (b). Schematic image showing the centre-line radius R (c). TQRs confining negative charge carriers in three cases of interest, vertically coupled with equal radii(d), concentric (e) and vertically coupled with different radii(f).

as the ratio between the upper and lower ring centre-line radii and β as the ratio between the inter-ring distance and R , explicitly these parameters can be written as follows:

$$R = \frac{R_{out} + R_{in}}{2}; \quad \alpha = \frac{R_2}{R_1}; \quad \beta = \frac{d}{R} \quad (2.5)$$

The TQRs in the present work can be placed with a specific radii ratio and interring distance, thus defining the following cases, vertically coupled TQRs of equal radii ($\alpha = 1, d \neq 0$), concentric rings ($\alpha \neq 1, d = 0$) and vertically coupled TQRs with different radii ($\alpha \neq 1, d \neq 0$) that is the most general case capable to reproduce the two first situations (Figs. 2.1(d), 2.1(e), 2.1(f) respectively).

The relative particle-particle distance in vertically coupled TQRs is an important geometrical

term since the Coulomb interaction depends explicitly on it. It is easy to show that can be written in cylindrical coordinates as:

$$|\vec{r}_2 - \vec{r}_1|^2 = \rho_1^2 + \rho_2^2 - 2\rho_1\rho_2 \cos(\varphi_2 - \varphi_1) + (z_2 - z_1)^2 \quad (2.6)$$

It has been defined with the purpose of facilitating the mathematical modeling, the particle vector positions respect to the system coordinate origin located at the lower ring symmetry center as follows:

$$\vec{r}_1 = \vec{R}_1(\varphi_1) + \vec{\rho}_{t_1}(\hat{e}_{t_1}); \quad \vec{r}_2 = \vec{R}_2(\varphi_2) + \vec{\rho}_{t_2}(\hat{e}_{t_2}) + \vec{d} \quad (2.7)$$

Where φ_k is the angle that defines the direction of vector \vec{R}_k over each centre-line, while the two-dimensional vector $\vec{\rho}_{t_k}$ identifies the particle position inside the CS.

In Fig.2.2(a) are schematically represented the vector quantities introduced in Eqs.(2.7) which allow to define a coordinate plane $X_{t_k} - Z_{t_k}$ (see Fig. 2.2(b)) on the ring CS, and its origin is coincident with the CS centroid. The aim of such transformation is to describe in a simplest way the particle motion along the CS using the well known adiabatic approximation, which is discussed in some detailed in the following section .

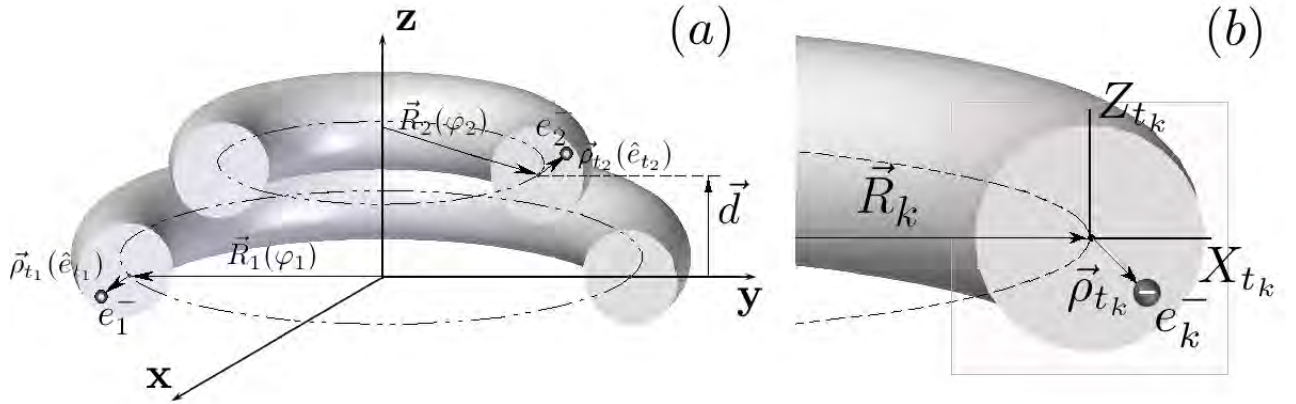


Figure 2.2: Redefinition of particles vector positions (a) and the $X_{t_k} - Z_{t_k}$ plane on the CS (b). It is worthwhile to notice this cartesian-like coordinate system is useful to analyze rectangular CSs while a polar transformation on this plane is needed to study circular CSs.

2.2 Adiabatic Approximation

The quantum mechanical description of many-particle systems has been a great deal of attention in computer science, physics, chemistry among other disciplines. Unfortunately finding exact stationary solutions of Schrödinger equation for such systems is virtually impossible. For instance, a diatomic molecule defines a very complex quantum mechanical system that involves two nuclei in motion and their surrounding electrons, and thus an approximate method to simplify the calculus of eigenstates and eigenenergies would be really useful.

The Born-Oppenheimer approximation [48] suggests that bearing in mind the fact that the mass of the electrons is much smaller than nuclei masses, then is possible to analyze the electrons and nuclei motions separately. The method begins neglecting the nuclei kinetic energy temporarily and the system Hamiltonian is solved for a fixed nucleus-nucleus distance r . Next from the set of eigenenergies obtained for this particular value of r , the ground state energy E_0 is taken and stored. The process continues similarly for different nucleus-nucleus separations, in such a way that finally the basal eigenenergy $E_0(r)$ can be build (at least numerically) as an explicit function of r (often referred as the potential energy surface (PES) [49]). The last step consists in including the $E_0(r)$ function as a confinement potential in the nuclei system Hamiltonian, and its solution leads to the eigenstates and eigenenergies of the diatomic molecule¹.

The first step represents the fact that the ground state remains as the state of the system for any nucleus-nucleus distance, emphasizing that r varies slowly as consequence of the nuclei masses. Physically this situation could be interpreted as if the electrons "follows adiabatically" the nuclei motion. In quantum mechanical terms, it means, that the system wavefunction adapts itself instantaneously to small changes of r .

For SAQD systems we assert the experimental fact observed by means of AFM, stating the mean radius is always greater in comparison with the height and ring thickness. According to the geometrical parameters defined in the previous section, it will be assumed that the torus CS is very narrow in comparison with the centre-line radius ($R_k \gg R_t$). This assumption will allows to decouple the fast transverse electron motion from the slow rotation motion around z-axis by using the adiabatic approximation.

¹The experimental data obtained for many quantum mechanical systems in the adiabatic regime, are in good agreement with the developed theory. In this sense, the adiabatic approximation constitutes a valid approximate solution method in quantum mechanics [37, 48].

In order to perform such decoupling, it is necessary to consider the transformations (2.7) that allows to rewrite the ρ_k cylindrical coordinate for each particle (see Fig.2.2(b)) as follows:

$$\rho_k = R_k + X_{t_k} \quad (2.8)$$

Furthermore, having into account the established fact that rings are very narrow, it leads to rewrite the system Hamiltonian (2.4) in this form:

$$\hat{H} = \sum_{k=1}^N \left[-\nabla_{t_k}^2 - \frac{1}{R_k^2} \frac{\partial^2}{\partial \varphi_k^2} - i\tau_k \gamma \frac{\partial}{\partial \varphi_k} + \frac{\gamma^2}{4} (R_k + X_{t_k})^2 + \hat{U}(\vec{r}_k) \right] + \hat{V}(|\vec{r}_2 - \vec{r}_1|) = E \quad (2.9)$$

Where $\nabla_{t_k}^2$ is the dimensionless kinetic energy operator related to the k th-particle motion on the $X_{t_k} - Z_{t_k}$ plane (this is, along the CS), while X_{t_k} is the X_t coordinate on the same plane. This form of Hamiltonian will allow us to model the several TQRs systems in the light of the adiabatic approximation, and will be used throughout the document.

Before to demonstrate the validity and the solution scheme implementing the adiabatic procedure in TQRs, an additional simplification in the Hamiltonian (2.9) can be done, by introducing the centre-of-mass and relative coordinates [38].

2.2.1 Centre-of-Mass and Relative Coordinates

The azimuthal particle motion is described thorough the φ_1 and φ_2 coordinates and basically they are related to the rotation motion around the z -axis as can be seen in Fig. 2.2(a). But by defining the relative and centre-of-mass coordinates given respectively by:

$$\varphi = \varphi_1 - \varphi_2 \quad (2.10a)$$

$$\theta = \frac{\varphi_1 + \alpha^2 \varphi_2}{1 + \alpha^2} \quad (2.10b)$$

It is possible to rewrite the Hamiltonian (2.9) for a system consisting of two identical particles as:

$$\hat{H} = \sum_{k=1}^N \left[-\nabla_{t_k}^2 + \frac{\gamma^2}{4} (R_k + X_{t_k})^2 + \hat{U}(\vec{r}_k) \right] - \frac{1}{R^2} \left(\frac{1}{\alpha^2} + 1 \right) \frac{\partial^2}{\partial \varphi^2} + \hat{V}(|\vec{r}_2 - \vec{r}_1|) - \frac{1}{R^2} \left(\frac{1}{\alpha^2} + 1 \right) \frac{\partial^2}{\partial \theta^2} - i\gamma \frac{\partial}{\partial \theta} \quad (2.11)$$

Where the φ and θ coordinates represent the relative and the centre-of-mass azimuthal motion around the symmetry axis of the two-particle system. The intention of using these coordinates is facilitating the process of solving the eigenvalue problem (2.9)².

The last two terms in (2.11) are acting on θ and none of the other terms depends on it. Therefore it can be used separation of variables and rewrite the Hamiltonian as follows:

$$\hat{H} = \hat{H}_a + \hat{H}_\theta \quad (2.12)$$

The term \hat{H}_θ can be related to the centre-of-mass azimuthal motion and explicitly is given by:

$$\hat{H}_\theta = -\frac{1}{R^2} \left(\frac{1}{\alpha^2 + 1} \right) \frac{\partial^2}{\partial \theta^2} - i\gamma \frac{\partial}{\partial \theta} \quad (2.13)$$

Whose exactly solvable eigenfunctions and eigenenergies are well known [38] and can be expressed respectively as follows:

$$\psi_\theta(\theta) = \frac{1}{\sqrt{2\pi}} e^{iM\theta} \quad (2.14a)$$

$$E_\theta = \frac{M^2}{R^2(\alpha^2 + 1)} + M\gamma \quad (2.14b)$$

Here, M is called the centre-of-mass angular quantum number and able to take the values $M = 0, \pm 1, \pm 2, \dots$. The remaining term \hat{H}_a contains the particle-particle interaction that depends on the rest of variables different from θ , and it is practically impossible to solve the eigenvalue problem by separation of variables, thus an approximate method is needed in order to find eigenstates and eigenenergies. In the next section it will set out some ideas that support the validity of using adiabatic approximation.

2.2.2 Model Validation

The Hamiltonian \hat{H}_a can be interpreted as the system Hamiltonian of five particles interacting through the potential \hat{V}_{int} which is the sum of confinement potential, the diamagnetic term and Coulomb interaction. This fact is clearly seen when we rewrite it as follows:

²It must be noticed that one-single particle systems do not require such coordinate transformation, so in this case the eigenvalue problem is relative easier because the number of degrees of freedom is smaller.

$$\hat{H}_a = \sum_{k=1}^N \left[-\frac{\partial^2}{\partial X_k^2} - \frac{\partial^2}{\partial Z_k^2} \right] - \frac{1}{R^2} \left(\frac{1}{\alpha^2} + 1 \right) \frac{\partial^2}{\partial \varphi^2} + \hat{V}_{int} \quad (2.15a)$$

$$\hat{V}_{int} = \sum_{k=1}^N \left[\frac{\gamma^2}{4} (R_k + X_{t_k})^2 + \hat{U}(\vec{r}_k) \right] + \hat{V}(|\vec{r}_2 - \vec{r}_1|) \quad (2.15b)$$

In Eq.2.15a, it is fundamental to notice the presence of five terms proportionally to energy kinetic operators which are related to five moving particles in the one-dimensional spaces X_1, X_2, Z_1, Z_2 and φ . Only with the purpose of showing the validity of using an adiabatic method, we will define a set of new coordinates that will map the $X_k - Z_k$ plane into another one $\bar{X}_k - \bar{Z}_k$ (see Fig.2.3). The rescaling transformation that describes the mapping process is given by:

$$X_k = \frac{w}{2} \bar{X}_k, \quad Z_k = \frac{l}{2} \bar{Z}_k \quad (2.16a)$$

Where w and l are the width and height respectively of a rectangular CS³. Consequently, by using this transformation, the Hamiltonian 2.15 can be finally rewritten as:

$$\hat{H}_a = \sum_{k=1}^N \left[-\frac{1}{\left(\frac{w}{2}\right)^2} \frac{\partial^2}{\partial X_k^2} - \frac{1}{\left(\frac{l}{2}\right)^2} \frac{\partial^2}{\partial Z_k^2} \right] - \frac{1}{R^2} \left(\frac{1}{\alpha^2} + 1 \right) \frac{\partial^2}{\partial \varphi^2} + \hat{V}_{int} \quad (2.17)$$

At this point, performing a comparison with the one-dimensional kinetic energy operator⁴, it is clear that Eq.2.17 can be understood as a Hamiltonian related to a five-particle system, where each one is moving independently in the corresponding $\bar{X}_1, \bar{X}_2, \bar{Z}_1, \bar{Z}_2$ and φ one-dimensional spaces, with masses proportional to $\left(\frac{w}{2}\right)^2$, $\left(\frac{l}{2}\right)^2$ and $\frac{1}{R^2}$. From here it follows, that the first four particles are lightweight and the last one is the heavier⁵ and they are interacting thorough the \hat{V}_{int} potential. Physically, the "lightweight particles" terms are related to the rapid motions described along the CS by the actual two particles in Z_k and X_k directions, which is a direct result of their "small masses". From a quantum mechanical point of view, this behavior is due to the reduced dimensions of the CS leading to a strong

³We took the rectangular section as an example, the analysis for a square CS is straightforward and in the case of a circular CS is quite similar.

⁴The kinetic energy operator for a particle with mass m^* in the x-direction is given by $\hat{T} = -\frac{\hbar^2}{2m^*} \frac{\partial^2}{\partial x^2}$

⁵Based on the fact that the CS dimensions are smaller than R ($w, l \ll R$).

confinement undergone by the particles, therefore, increasing significantly their kinetic energies⁶ giving rise to fast motions along the CS.

In short, the Eq.2.15 can be reinterpreted as the system Hamiltonian consisting in four lightweight particles and one heavy particle interacting by means of the potential \hat{V}_{int} (an analog system such the diatomic molecule presented above with lightweight electrons and heavier nuclei in motion), whose masses can be adjusted by modifying the w , l , and R geometrical parameters characteristic of the TQRs systems.

It must be noticed that this section had only the objective of supporting the validity of using the adiabatic approximation, thus the transformations defined above will no be longer used in the rest of he document. In the subsequent section, it is presented schematically an algorithm that allows to solve the \hat{H}_a Hamiltonian in the adiabatic regime.

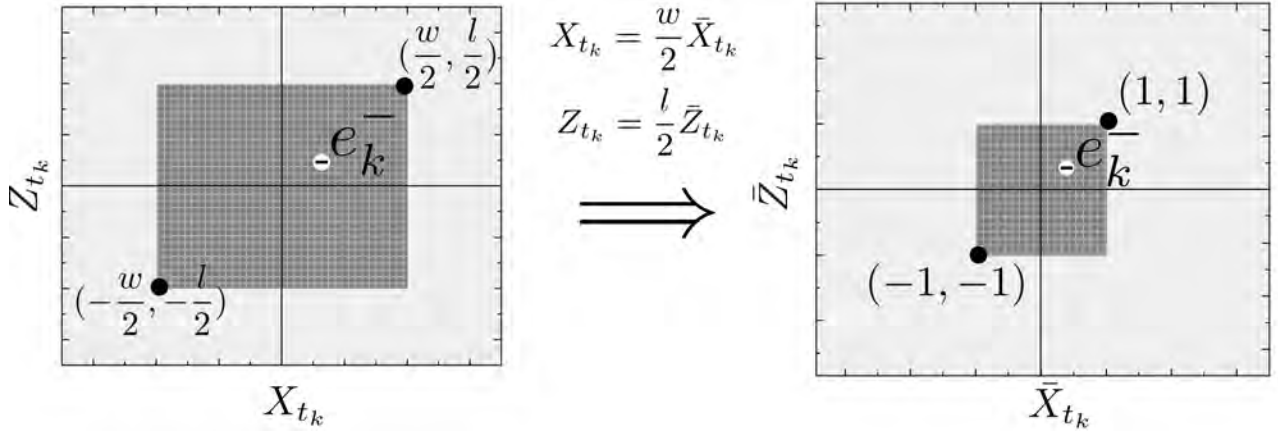


Figure 2.3: $X_{t_k} - Z_{t_k}$ plane mapping into the the $\bar{X}_{t_k} - \bar{Z}_{t_k}$ plane. In the former plane, the particles (electrons for instance) are constrained to move into a rectangle with sides l and h ($-\frac{w}{2} \leq X_{t_k} \leq \frac{w}{2}$ and $-\frac{l}{2} \leq Z_{t_k} \leq \frac{l}{2}$), on the other hand, in the latter, they are moving inside of a square of half side equal to one ($-1 \leq \bar{X}_{t_k} \leq 1$ and $-1 \leq \bar{Z}_{t_k} \leq 1$).

⁶The Heisenberg uncertainty principle in one dimension ($\Delta x \Delta p_x \geq \frac{\hbar}{2}$) predicts that the kinetic energy uncertainty ($\frac{\Delta P_x^2}{2m^*}$) is proportional to the inverse square position uncertainty. Thus, in the context of TQRs, as the CS dimensions are reduced, it gives rise to a high degree of localization of the wavefunctions (by reducing Δx) and simultaneously the quantity $\frac{\Delta p_x^2}{2m^*}$ related to the kinetic energy, is increased substantially.

2.2.3 Solution algorithm using adiabatic approximation

According to Born-Oppenheimer ideas, the system wavefunction can be expressed as the product of two wave functions corresponding to the rapid motion over the CS and another one that describes the slow rotation motion around the symmetry axis⁷:

$$\psi_{RS}(\vec{r}) = \psi_R(X_1, X_2, Z_1, Z_2, \varphi)\psi_S(\varphi) \quad (2.18)$$

Then, the method begins fixing a value of φ and solving the eigenvalue problem provided by Eq.2.15:

$$\left[\sum_{k=1}^N \left[-\frac{\partial^2}{\partial X_k^2} - \frac{\partial^2}{\partial Z_k^2} \right] + \hat{V}_{int} \right] \psi_R(X_1, X_2, Z_1, Z_2, \varphi) = E_\varphi \psi_R(X_1, X_2, Z_1, Z_2, \varphi) \quad (2.19)$$

Here, E_φ denotes the eigenenergies obtained for that particular value of φ . The process of solving Eq.2.19 is continued for several values of φ until the function $E(\varphi)$ ⁸ can be expressed explicitly as a function of φ (in general numerically) from a set of tabulated values (φ , E_φ). The next step in the method consists in introducing the PES function as a confinement potential for the "heavier particle" system Hamiltonian giving rise to the eigenvalue problem:

$$\left[-\frac{1}{R^2} \left(\frac{1}{\alpha^2} + 1 \right) \frac{\partial^2}{\partial \varphi^2} + E_\varphi \right] \psi_S(\varphi) = E_{RS} \psi_S(\varphi) \quad (2.20)$$

Where the eigenvalues E_{RS} obtained by solving the latter Hamiltonian according to the adiabatic approximation, correspond to the eigenenergies of the whole system (lightweight and heavy particles). It is very important to notice that we previously separated the centre-of-mass angular motion, thus the desired complete two-particle system eigenfunctions and eigenvalues are finally expressed as:

$$\Psi(\vec{r}) = \psi_R(X_1, X_2, Z_1, Z_2, \varphi)\psi_S(\varphi)\psi_\theta(\theta) \quad (2.21a)$$

$$E = E_\theta + E_{RS} \quad (2.21b)$$

It is worthwhile to stress in the fact that despite of using an approximate method, additional computational challenges arise when solving the eigenvalue problems (2.19, 2.20), in general it is necessary to have to recourse to numerical methods. In the present work with the goal to guarantee that the methods converge, it is assumed that the CS dimensions to centre-line

⁷The appearance of ψ_θ is being neglecting temporally in order to get the \hat{H}_a solution into focus

⁸The PES function related to this system

radius aspect ratio is small and the magnetic field is not very intense. In the next subsection it is analyzed the system Hamiltonian of two particles in quantum rings in presence of on-axis donors, which is also possible to be solved in light of the adiabatic approximation by adding the Coulomb interactions between the particles and the donors to the potential term \hat{V}_{int} given by the Eq.2.15b.

2.2.4 Quantum rings and donor impurities

A subject of extensive theoretical and experimental studies has been the analysis of quantum rings in presence of impurities [23, 24]. The aroused curiosity is due to additional morphological and physical properties exhibited by these systems that could lead to tailor more complex energy spectra since they are strongly dependent on parameters such as the location and type of impurities used, and consequently offering the possibility of developing new devices and applications. As will be show in chapter 6, the energy spectra of these nanostructures exhibit singular properties and that is the reason because they are often called artificial molecules [34].

In the present work we consider two on-axis donor impurities located at the positions $\vec{a} = (0, 0, a)$ and $\vec{b} = (0, 0, -b)$. The dimensionless Hamiltonian 2.4 is then modified by adding the terms corresponding to the particles-donors (added terms within the summation operator) and donor-donor (\hat{V}_{ii}) interactions. Thus the two-particle Hamiltonian in presence of two on-axis impurities can be written as:

$$\hat{H} = \sum_{k=1}^N \left[-\nabla_k^2 - i\tau_k \gamma \frac{\partial}{\partial \varphi_k} + \frac{\gamma^2}{4} \rho_k^2 + \hat{U}_k(\vec{r}_k) + \frac{2\tau_k}{|\vec{r}_k - \vec{a}|} + \frac{2\tau_k}{|\vec{r}_k - \vec{b}|} \right] + \hat{V}(|\vec{r}_2 - \vec{r}_1|) + \hat{V}_{ii} \quad (2.22a)$$

$$\hat{V}_{ii} = \frac{2}{|\vec{a} - \vec{b}|} \quad (2.22b)$$

As it will be shown later, the Hamiltonian 2.22a is the most versatile model since it is possible to obtain for example, a two-electron system in two vertically coupled toroidal rings as a limiting case by moving away systematically the on-axis donor locations. In this sense, considering these kind of molecular complexes leads to a more general and interesting situations.

Finally, in the following section will be described briefly the methods and the computational tools used for solving the systems to be exposed in the subsequent chapters.

2.3 Numerical methods and computational tools

With the advent of computing technology, nowadays are available many programming environments offering different advantages, such as the possibility of creating modular programs and reusable source code⁹, platform-independent¹⁰, multithreaded¹¹ among others [50]. The crucial point here, is selecting an adequate environment to run efficiently numerical calculations in sequential steps using the less machine resources as possible (although for example, the modern technology processors can perform complex calculations efficiently, almost independently on the number of double precision variables used in the program). By this reason FORTRAN is an ideal environment according to this purpose, and the main advantage is there is a considerable amount of powerful scientific oriented software, programs and subroutines available for which there is no equivalent in a modern language.

The numerical analysis involved in this work, implemented the SPLINE¹² and QUANC8¹³ subroutines in order to perform numerical interpolation and integration procedures, respectively [51]. Additionally was imported the BESSELIB library, that provides Bessel-type functions and their derivatives useful in the TQRs with circular CS analysis. Finally, in order to solve eigenvalue problems, it was implemented a more complex program that performs a numerical method receiving the name of trigonometric sweep method [52], which was written in FORTRAN77 and has been successfully used in several theoretical works [27, 34]. In Appendix A is explained this method in some detail focusing on some important characteristics of TQRs systems.

In the following chapter it is presented a set of two-electron systems confined to move into strict one-dimensional rings, thus the system Hamiltonian is simplest to solve and there is no need to implement an approximate method, by this reason they are often called quasi-exactly solvable systems.

⁹These concepts are often implemented in the oriented object programming environments, allowing to write very compact source code and subsequently reuse it, creating objects from it

¹⁰Property that allows to run the same program on different systems and machines.

¹¹Capability of performing several tasks simultaneously within a main program.

¹²The spline method is an interpolation procedure where a function is fitted using piecewise polynomials called splines

¹³The Quanc8 method is a numerical integration technique which name is derived from quadrature adaptive Newton-Cotes's 8 panel. The Newton-Cotes formulas are a family of quadrature rules that are obtained by integrating interpolated polynomials over equally spaced evaluation points.

Chapter 3

One-dimensional quasi-exactly solvable systems

The fabrication of self-assembled quantum rings obtained by Lorke and co-workers [25] has motivated a great number of studies both theoretical and experimental. The knowledge of the energy structure related to these mesoscopic systems becomes essential for their potential application in opto-electronic devices. Recently, it has been reported the fabrication of two vertically stacked nanorings (VSN) [53] that offer great advantages in comparison with one-single quantum rings, due to the separation between rings which provides an additional degree of freedom. This fact can be used to configure the carrier energy structure with the aim of fabricating novel devices and studying mesoscopic physics related to interesting phenomena such as the Aharonov-Bohm effect [54] and persistent currents [54]. However, the most important use for these vertically coupled rings is related to the possibility of analyzing the electronic correlation effects and their influence on the energy spectrum. In this sense a two-electron system (TES) has been used because it provides an excellent testing ground for the several approximate methods developed to study the correlation effects. For this purpose, different theoretical approaches have been used to analyze the two-electron problem, such as the quantum Monte Carlo technique [55], renormalized perturbation theory [56], and other numerical methods [52]. In spite of these methods give excellent results they require great computational and mathematical efforts in order to obtain reliable results. In order to simplify the hard calculations related to the two electron energy structure, a one-dimensional exactly solvable model which describes their rotation around the z-axis in presence of a magnetic field recently has been proposed [26]. This model corresponds to a ring with infinite barrier potential and infinite radius-to-width aspect ratio. This TES is very important since there are not many exactly solvable problems in quantum mechanics. Nevertheless, it is necessary to emphasize that the single one-dimensional ring is a very restrictive configuration

because makes impossible that the azimuthal coordinates related to the orbital motion of the electrons, take an equal value. Additionally, in these one dimensional rings [26] is not possible to study the attractive interactions between particles with different charges such as an electron-hole pair due to the Coulomb interaction in one dimensional space is unstable. In order to avoid these problems it is proposed a system compound by two VSN with different radii each one confining only one single electron. By means of an adequate selection of the radii ratio and the interring distance is possible to reproduce an exact form of the results reported in Ref. [26, 27].

3.1 System Hamiltonian

The model considered is compound by two spatially separated electrons which are forced to rotate into two VSN which have infinite radius-to-width aspect ratio. The system in presence of an uniform magnetic field \vec{B} which is oriented along the z-axis (the system symmetry axis) (see Fig. (3.1)). The radii of the rings, the interring distance, the α and β parameters are the same discussed in the section 2.1.2. In order to compare our results with those obtained in [26, 27], it has been used the same notation and units considered in the section 2.1.1. The two-particle renormalized dimensionless Hamiltonian $\tilde{H} = \hat{H}R^2$ can be expressed in cylindrical coordinates as:

$$\tilde{H} = \sum_{k=1}^2 \left[-\nabla_k^2 - i\gamma \frac{\partial}{\partial \varphi_k} + \frac{\gamma^2 R_k^2}{4} + \hat{U}_k(\vec{r}_k) \right] R^2 + \hat{V}(|\vec{r}_2 - \vec{r}_1|) R^2 \quad (3.1)$$

Eigenvalues of the Hamiltonian 3.1 corresponding to the renormalized two-electron energies $\tilde{E} = ER^2$ (being E the eigenenergies of \hat{H}) can be found exactly by using the center-of-mass and relative coordinates. In these coordinates, the Hamiltonian 3.1 can be rewritten as $\tilde{H} = \tilde{H}_\varphi + \tilde{H}_\theta$ where \tilde{H}_θ and \tilde{H}_φ are respectively the center-of-mass and relative terms which can be written as:

$$\tilde{H}_\theta = -\frac{1}{\alpha^2 + 1} \frac{\partial^2}{\partial \theta^2} - i\gamma R^2 \frac{\partial}{\partial \theta} + (\alpha^2 + 1) \frac{\gamma^2 R^4}{4} \quad (3.2)$$

$$\tilde{H}_\varphi = -\left(\frac{1}{\alpha^2} + 1\right) \frac{\partial^2}{\partial \varphi^2} + \frac{2R}{\sqrt{1 + \alpha^2 - 2\alpha \cos(\varphi) + \beta^2}} \quad (3.3)$$

The exact eigenvalues of the operator 3.2 are given by:

$$\tilde{E}_\theta = \left(\frac{M}{(\alpha^2 + 1)^{1/2}} + \frac{(\alpha^2 + 1)^{1/2} \gamma R^2}{2} \right)^2 \quad M = 0, \pm 1, \pm 2 \dots \quad (3.4)$$

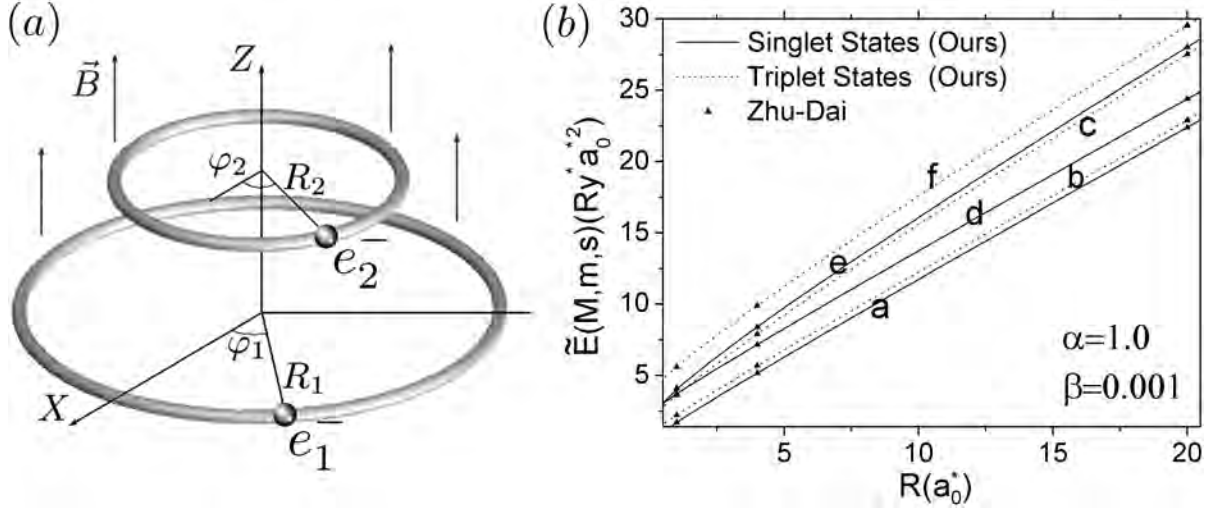


Figure 3.1: One dimensional vertically coupled nanorings geometry (a). Comparison between the values of renormalized energy obtained in the vertically coupled rings configuration and those reported in [26] (b).

On the other hand, the eigenvalues of the operator 3.3 as $E_\varphi(m, s)$ are determined by solving numerically the eigenvalue problem 3.5a with periodic boundary conditions in the region $[-2\pi, 2\pi]$ defined by 3.5b:

$$\tilde{H}_\varphi \psi_{m,s}(\varphi) = \tilde{E}_\varphi(m, s) \psi_{m,s}(\varphi) \quad (3.5a)$$

$$\psi_{m,s}(-\varphi) = (-1)^s \psi_{m,s}(\varphi); \quad \psi_{m,s}(\varphi)(-1)^M = \psi_{m,s}(\varphi \pm 2\pi) \quad (3.5b)$$

Where the quantum number $m = 0, \pm 1, \pm 2$ defines the two-electron relative angular momentum and $s = 0, 1$ defines the eigenfunction parity. The even solutions ($s = 0$) and the odd ones ($s = 1$) correspond respectively to singlet and triplet states as explained in Appendix A. Therefore the TES energy spectrum can be expressed as following:

$$\tilde{E}(M, m, s) = \tilde{E}_\theta(M) + \tilde{E}_\varphi(m, s) \quad (3.6)$$

In order to check of the precision of this numerical procedure, it has been performed the calculations of a part of some low-lying states in the limiting case when simultaneously α tends to one and β tends to zero. The results obtained are shown in Fig. 3.1(b), where it can be seen that exact values corresponding to black triangle symbols [26] are very close to the solid curves obtained by the TES in vertically coupled rings model. This fact is an indirect

demonstration of the good quality of the results obtained by the versatile model proposed in the present work which considers two electrons spatially separated.

3.2 Wigner Crystallization in one-dimensional vertically coupled rings

The normalized total energy as a function of R is displayed in Fig. 3.2 (a). From this figure is concluded that the energy spectrum is very sensitive to the changes of the geometrical parameters since the greater the ring radius the greater is the renormalized energy. It is due to the renormalized potential energy is directly proportional to the ring radius while the renormalized kinetic energy is independent of the radius. For this reason for small values of the ring radius, the kinetic energy dominates on the potential energy which yields to a variation of the curves slope. On the other hand, for greater ring radius the potential energy dominates on the kinetic energy and this fact is evident because the slope becomes constant. This result can be interpreted as a transition between like-gas systems to an ordered system, similar to a Wigner crystal.

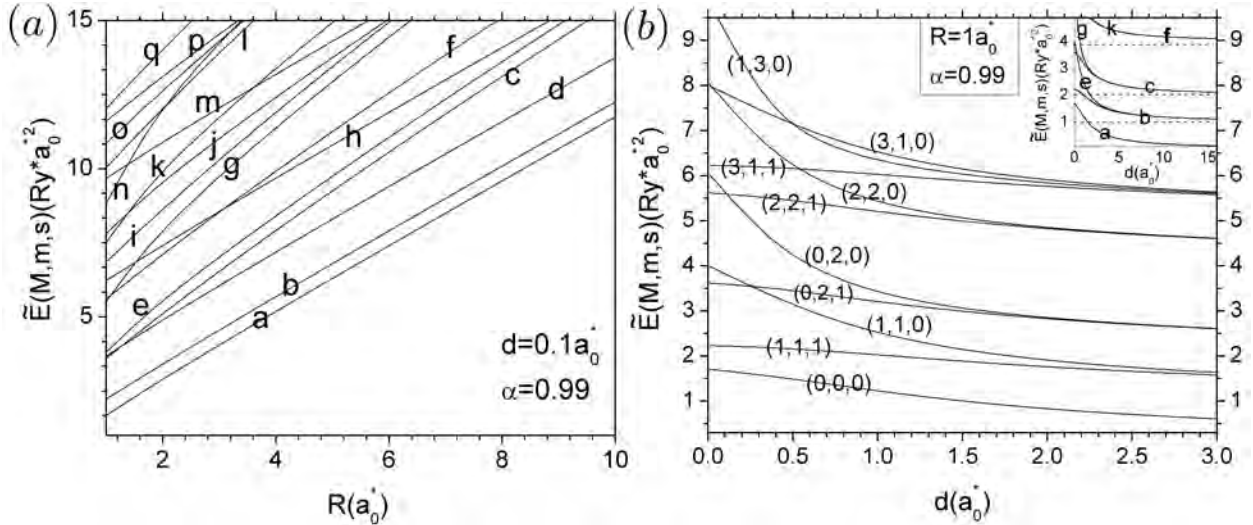


Figure 3.2: Normalized total energy as function of R for a small interring distance $d = 0.1a_0^*$ (a) and as function of d for $R = 1a_0^*$ (b).

From Fig. 3.2(b) it can be seen indirectly that the double ring system becomes to behave as a non interacting two-electron system when the interring distance is increased. This fact

it is confirmed by the superposing of some of the energy states (for instance the (0,2,1) and (0,2,0) states) in the energy spectrum for interring-distances greater than $2a_0^*$, becoming these states almost indistinguishable in the figure. A similar effect occurs in a crystal lattice when the inter-atom distance is increased. In crystalline structure compounds of N atoms, the atomic single energy states are superposed due to their proximity giving rise to the energy bands of the solid. But when they are moved away enough among them, the energy states are not longer superposed, thus it is obtained an energy spectrum formed by only the single energy levels related to N isolated atoms (where every energy has a degeneracy equal to N) [6]. This interesting characteristic confirms the influence of the interactions among particles in nanostructures.

Furthermore, from Fig. 3.2 (b) it can be seen that the energy of the states (M, m, s) for large inter-ring distances converges to the exact values of the renormalized energy for a two non-interacting particles in two identical and vertically stacked nanorings, which is easy to show is given by $\tilde{E}_{non-inter} = (M^2 + m^2)/2$. In the inset of this figure, it is shown more clearly the tendency for larger values of d .

Finally, it is important to mention that this situation can be used as criterion for establishing the critical inter-ring distance in which they are decoupled, thus obtaining a system of two single rings and electrostatically decoupled. In light of this criteria, could be affirmed in the situation presented in the Fig. 3.2 (b), that for interring distances greater than $3a_0^*$, there is a strong degree of uncoupling between the two rings because of the reasons mentioned above.

3.3 Aharonov-Bohm effect in one-dimensional vertically coupled rings

In figures 3.3 it is shown the evolution of the two-electron energy spectrum with the renormalized magnetic field (γ) applied along the common symmetry axis. It has been considered four values of the radii ratio: $\alpha = 0.8, 0.99, 1.05, 1.2$. In order to understand these curves is necessary to take into account that they are a result of the strong competition between two terms. The first of them is the diamagnetic term which is proportional to the square magnetic field while the second one, the paramagnetic term, changes linearly with the magnetic field. For this reason, for small values of the magnetic field all curves are approximately linear but when the magnetic field is increased, the curves present a parabolic behavior with positive slope as $M > 0$ and a negative slope as $M < 0$.

In these curves, the Aharonov-Bohm oscillations corresponding to the periodic alternation of the spin related to the ground state are strongly dependent on the radii ratio, as it can be seen the greater the radii ratio the smaller is the period of the Aharonov-Bohm oscillation. The period for $\alpha = 0.99$ and $\alpha = 1.05$ (it means that the radii of the rings are very close) the period is equal to 1.01 and 0.95 respectively, while this period becomes equal to 1.21 and 0.81 as the α parameter is equal 0.8 and 1.2, respectively. These values of the period can be obtained from the analytic expression $T = 2/(R^2(1 + \alpha^2))$ easily obtained from the Eq. 3.6. The critical γ values which minimize the total renormalized energy satisfy the relation $\gamma_{critical} = 2M/((\alpha^2 + 1)R^2)$ and the corresponding minima value of the energy is $\tilde{E}_{min} = \tilde{E}(M, m, s)|_{\gamma_{critical}} = \tilde{E}_r(m, s)$.

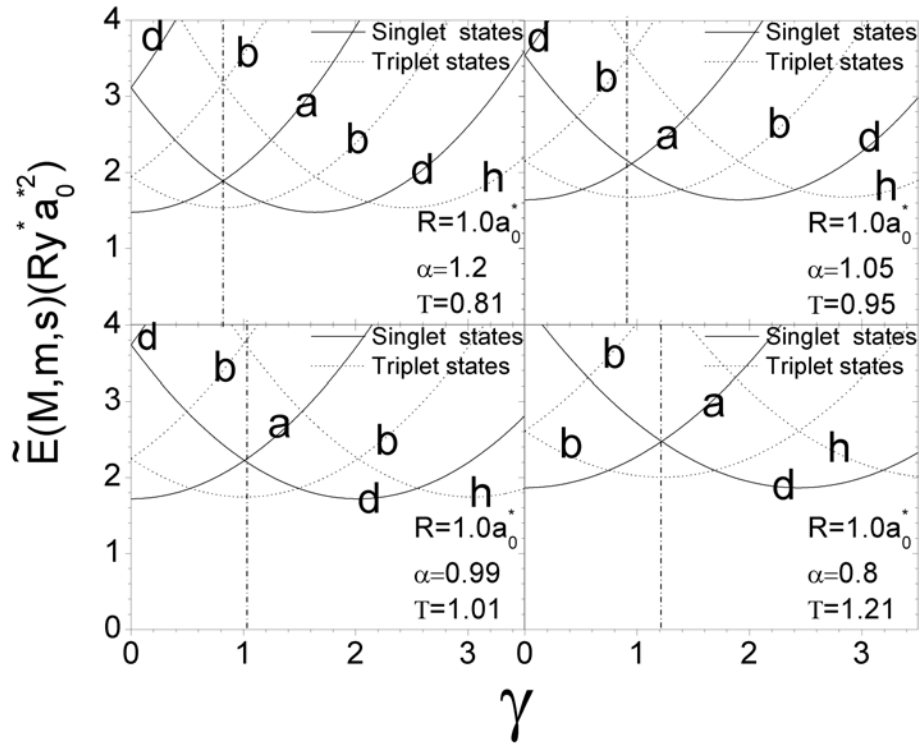


Figure 3.3: Renormalized total energy as function of γ parameter. The Aharonov-Bohm effect clearly appears as the oscillatory and periodic spin-shift for the ground state when the magnetic field strength is increased, giving rise to transitions in the sequence singlet-triplet-singlet. The period of this oscillations is modifiable by changing the ring radius or the radii ratio.

3.4 Size effect on the one-dimensional vertically coupled rings spectrum

In order to determine which geometrical parameters have a greater influence on the two-electron energy spectrum, it has been calculated a set of data for displaying a three dimensional curve for the ground state energy as function of the radii ratio and the interring separation (see Fig. 3.4 (a)). In order to facilitate the analysis, it has been also plotted the contour curves (Fig. 3.4 (b)). From the former curve, it can be seen that ground state is more sensitive to variations of the radii ratio than the variations of the separation between rings. This fact is easier to be observed from the contour curves, since the separation between two contour curves is smaller (thus the variation in the slope is more noticeable) along the α axis than along the β axis. This effect can be magnified as the magnetic field becomes different to zero, since diamagnetic term is strongly dependent on the α parameter.

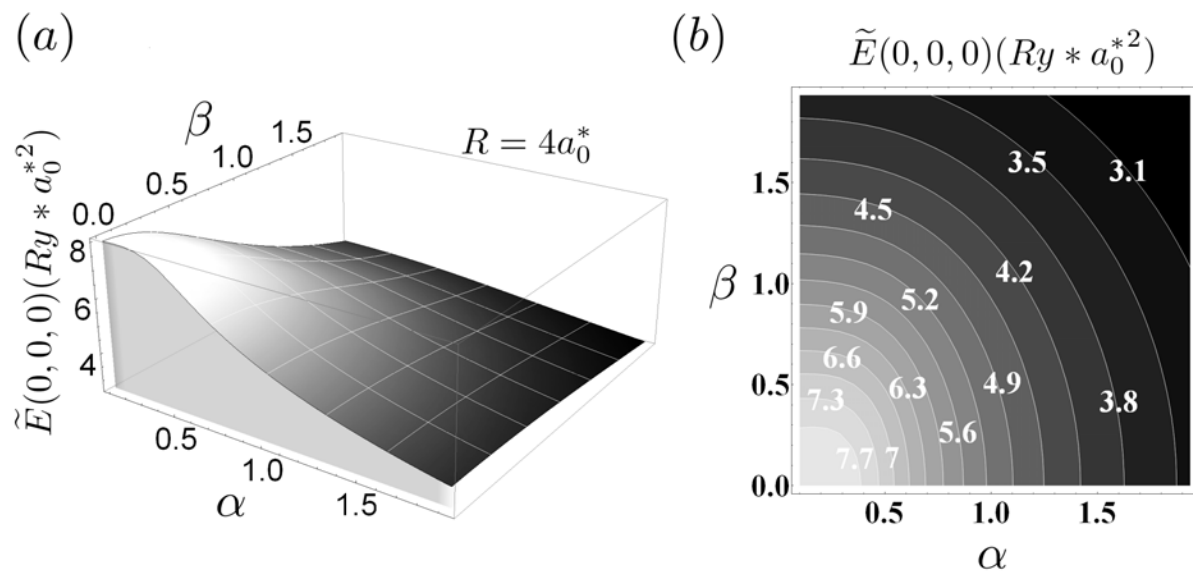


Figure 3.4: Renormalized total energy as function of the α and β parameters (a). Contour curves for the renormalized total energy as function of the α and β parameters. A value of $R = 4a_0^*$ was used for these curves.

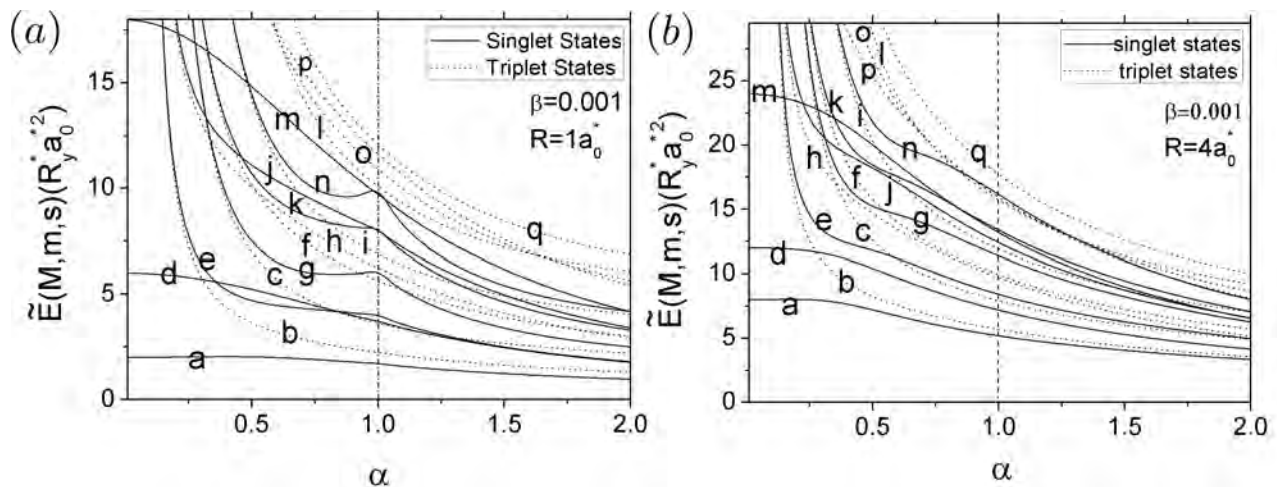


Figure 3.5: Renormalized energy as a function of the radii ratio as the greater radius is equal to $1.0a_0^*$ (a) and equal to $4.0a_0^*$ (b). In both cases, the two rings are very close by using a β value of 0.001.

In figures 3.5 it is shown a part of energy spectrum as a function of the radii ratio for two fixed values of R parameter, $R = 1.0a_0^*$ (Fig. 3.5 (a)) and $R = 4.0a_0^*$ (Fig. 3.5 (b)). It can be seen the existence of a little peak for some singlet states as the radii ratio tends to one, which means that the rings tends to merge in only one ring. In order to give an explanation of this fact, is necessary to take into account that electrons in singlet states are forced to take opposing positions with the aim of avoiding the violation of the fundamental Pauli's principle. In this case, the renormalized total energy increases due to the reduction of the electron-electron separation. However, this effect suffers a quenching when the radius increases as can be seen in Fig. 3.5 (b), which is a consequence of diminishing the potential energy. Finally the states a, d , and m which have the same relative angular momenta quantum number $m = 0$, in the limiting case when α tends to zero, their energy values converges to the corresponding quantum rigid rotor renormalized energy value $\tilde{E}_{Rotor} = M^2 + 2R$.

Chapter 4

Two-dimensional systems

4.1 Two-particle systems in Nanoribbons

The study of the energy spectrum of particles confined in quantum systems with cylindrical symmetry has generated a great deal of attention since the first reports of carbon nanotubes [57]. Recently, V. Prinz [58, 59] has experimentally established the possibility of fabricating semiconductor nanotubes, which can be obtained from two different semiconductors with a lattice parameter mismatch up to 7%. This discontinuity inextricably yields strain effects during the epitaxial growth, in such way that an overgrowth can lead to a stress relaxation due to the reduction of the elastic energy. In consequence, the structure spontaneously is rolled-up over itself adopting a tube shape. This tube-shaped semiconductor structure is characterized by its thickness, height and diameter which are strongly dependent on the initial semiconductor bilayer width as well as the stress mechanism generated as a consequence of the mismatch parameter. The crucial point of this report is related to the possibility of fabricating quasi-two-dimensional cylindrical ribbons by tailoring their geometrical parameters by means of a controlled growth process. These semiconductor nanotubes display remarkable features in comparison with those made from carbon. For instance, the semiconductor nanotubes have a diameter much greater than the carbon nanotubes and its curvature is more regular. In this sense, the cylindrical semiconductor nanostructures become more suitable for potential applications due to the strong relation between nanotube diameter and "magnetic field length" [60, 61] which allows to achieve a great control on the carrier quantum states. This fact has been demonstrated both theoretically and experimentally [60] by considering only one electron into the single semiconductor nanotube [61]. The results have shown fundamental differences related to electrical current distributions generated in cylindrical and planar structures. Despite the importance of this study [61], it is considered also interesting to analyze the case of two particles constrained to move into two dimensional

cylindrical ribbons, since allows to study the electron-electron correlation and the influence on the energy spectrum in two-dimensional spaces. Furthermore, it is desired to explore the influence of the geometrical parameters on the energy structure of such two-particle system. It is important to emphasize that the knowledge of the electronic properties and their control are crucial subjects in the purpose of realizing both technological applications and studies of mesoscopic physics [62] such as the Aharonov-Bohm effect and the persistent currents. Motivated by finding new physical effects in two dimensional ribbons with cylindrical symmetry, in this chapter, it is analyzed the energy spectrum of two particle spatially separated in two cylindrical quantum ribbons. Nanostructures concentrically coupled have been studied previously [41] in ring-shaped quantum dots in which their thickness and height are very small in comparison with their mean radii. Additionally, it is study the energy spectrum of one and two-particle systems constrained to move into a two-dimensional flat-ring in presence of ionized impurity donors and a static and uniform magnetic field. Finally, it is analyzed the geometry influence of the two-dimensional systems studied in this chapter, on the Aharonov-Bohm oscillations period.

4.1.1 System Hamiltonian

The model considered essentially consists of two particles which are constrained to move into two coaxial cylindrical nanoribbons with z-axis as the system common axis. Both cylindrical shells have the same height h and inner and outer ribbons have radii equal to $R_1 = R$ and $R_2 = \alpha R$, respectively, being α a dimensionless parameter which allows to consider the effect of the radii ratio of the ribbons on the energy spectrum. It is expected that as the radii ratio tends to one ($\alpha \rightarrow 1$) and the ribbons' height tends to zero ($h \rightarrow 0$), the results must coincide with those previously reported in the Ref. [26, 27] for two particles in a single one-dimensional ring. A schematic picture of the two particles into two concentric ribbons under an homogeneous magnetic field oriented along the symmetric axis is shown in Fig. 4.1. By using the effective-mass approximation, the energy labeling notation described in Appendix B and the units treated in the section 2.1.1, the dimensionless renormalized Hamiltonian for the system under analysis can be written in cylindrical coordinates $\vec{r}_k(\rho_k, \varphi_k, z_k)$, $k = 1, 2$ as:

$$\tilde{H} = \hat{H}R^2 = \sum_{k=1}^2 \left[-\nabla_k^2 - i\gamma \frac{\partial}{\partial \varphi_k} + \frac{\gamma^2 R_k^2}{4} + \hat{U}_k(\vec{r}_k) \right] R^2 + \hat{V}(|\vec{r}_2 - \vec{r}_1|) R^2 \quad (4.1a)$$

$$\hat{V}(|\vec{r}_2 - \vec{r}_1|) R^2 = \frac{2R}{\sqrt{1 + \alpha^2 - 2\alpha \cos(\varphi_1 - \varphi_2) + \left(\frac{z_1 - z_2}{R}\right)^2}} \quad (4.1b)$$

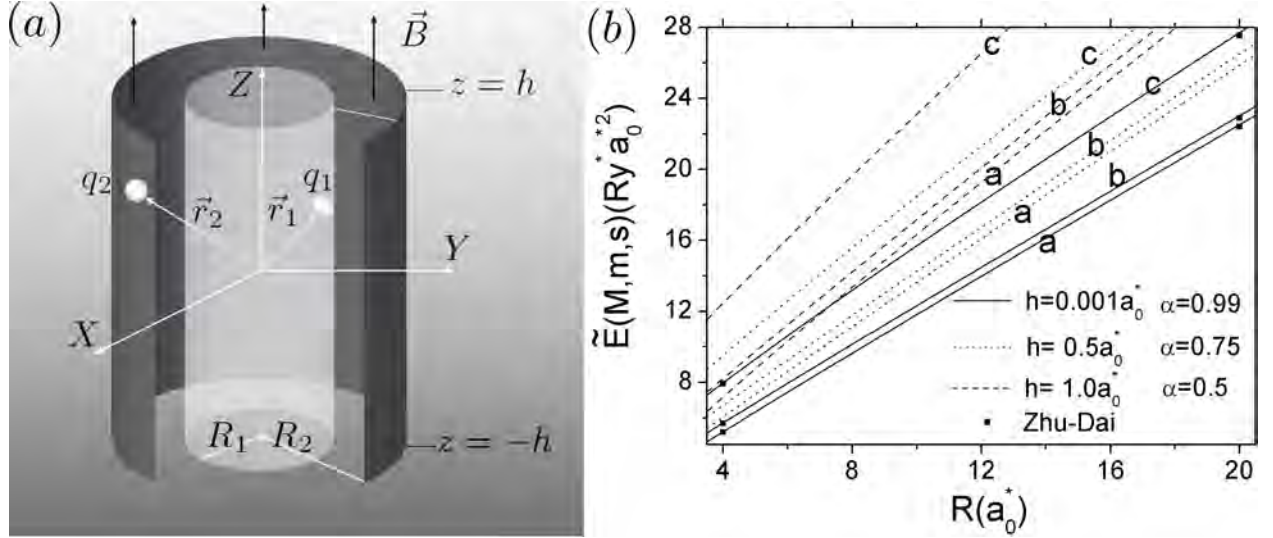


Figure 4.1: Schematic picture of two particles in two coaxial nanoribbons under an homogeneous magnetic field(a). Normalized energies for the states $a(0, 0, 0)$, $b(\pm 1, 1, 1)$ and $c(0, 2, 1)$ as a function of the ribbon's inner radius. The solid square symbols correspond to the values obtained by an exact method, for two electrons in one-dimensional ring. The lines for different values of α (0.5, 0.75, 0.99) and h (1.0, 0.5, 0.01) a_0^* are the results obtained in the present work (b).

Where $\hat{V}(|\vec{r}_2 - \vec{r}_1|)R^2$ is the renormalized Coulomb potential. Motivated by the possibility of comparing the obtained results in this research with those previously reported for limiting cases in [26, 27, 62, 41, 63], it is analyzed in light of the adiabatic approximation, very narrow nanoribbons with small height-to-base aspect ratio. Under this condition, $h/R \ll 1$, this method allows to decouple the fast particle motion in z -direction from the slow particle rotation motion around the z -axis. By means of consistent application of the adiabatic approximation, the two-particle Hamiltonian 4.1a can be written as:

$$\tilde{H} = -\left(\frac{\partial^2}{\partial\varphi_1^2} + \frac{1}{\alpha^2}\frac{\partial^2}{\partial\varphi_2^2}\right) - i\gamma R^2\left(\tau_1\frac{\partial}{\partial\varphi_1} + \tau_2\frac{\partial}{\partial\varphi_2}\right) + \frac{\gamma^2 R^4(1 + \alpha^2)}{4} + \bar{V}_{eff}(\varphi_1 - \varphi_2) \quad (4.2a)$$

$$\bar{V}_{eff}(\varphi) = \frac{\langle f_1^0 f_2^0 | \hat{V}(|\vec{r}_2 - \vec{r}_1|) R^2 | f_1^0 f_2^0 \rangle}{\langle f_1^0 f_2^0 | f_1^0 f_2^0 \rangle} \quad (4.2b)$$

The quantity $\bar{V}_{eff}(\varphi)$ is denoted as the mean effective potential, calculated from the one-

particle ground state wave functions $f_k^0 = f_k^0(z_k)$ $k = 1, 2$ which are related to a particle in a one dimensional infinite quantum well of width equal to $2h$. By using the center-of-mass and relative coordinates the two-particle Hamiltonian 4.2a can be separated into center-of-mass, \tilde{H}_c and relative \tilde{H}_r terms as follows

$$\tilde{H}_\theta = -\left(\frac{1}{\alpha^2 + 1}\right) \frac{\partial^2}{\partial \theta^2} - i\gamma R^2 \frac{\partial}{\partial \theta} + (\alpha^2 + 1) \frac{\gamma^2 R^4}{4} \quad (4.3a)$$

$$\tilde{H}_\varphi = -\left(\frac{1}{\alpha^2 + 1} + 1\right) \frac{\partial^2}{\partial \varphi^2} + \bar{V}_{eff}(\varphi) \quad (4.3b)$$

The solution algorithm follows the same steps stated in chapter 3, the renormalized energy is calculated as $E(M, m, s)R^2 = \tilde{E}(M, m, s) = \tilde{E}_\theta(M) + \tilde{E}_\varphi(m, s)$ where $\tilde{E}_\theta(M)$ are calculated exactly from the Hamiltonian 4.3a and $\tilde{E}_\varphi(m, s)$ are the numerical eigenvalues of the problem given by the Hamiltonian 4.3b.

For comparison purposes, it has been calculated systematically the evolution of the normalized energies of the first three low-lying states as a function of the inner radius R with some different pairs of values of the radii ratio and height of ribbons (see Fig. 4.1(b)). The chosen values for α are close to one ($\alpha = 0.5, 0.75, 0.99$), while those of h are close to zero ($h = 1.0, 0.5, 0.01a_0^*$). A glance on the curves for electrons spatially separated in two coaxial nanoribbons, allows to conclude that energy values obtained numerically (in lines) consistently tend to those ones obtained in [26] (black square symbols) for a two-electron system in a single one-dimensional ring.

Physically it means that, as the radii ratio α tends to one and the ribbon's height h to zero, the proposed model of concentric ribbons shows that the under these conditions nanoribbons gradually merges forming a structure similar to a one single ring confining two electrons. This remarkable fact is a direct confirmation of the high quality of the results obtained which were reconfirmed with the calculation of a broader set of energy levels as it is shown in Table 4.1.

Additionally, it can be seen that the two-electron energy spectrum is strongly dependent on the geometrical parameters. For instance, all energy levels with inner radius equal to $4a_0^*$ are smaller than those with inner radius equal to $20a_0^*$. The same behavior is seen as the radii ratios increase and the ribbon's height decrease. It is due to the renormalized potential energy is directly proportional to inner radius meanwhile is inversely proportional to the square root of h .

Table 4.1: Comparison between exact energy values corresponding to [26] and the energy values obtained for two electrons in two concentric quantum ribbons for a set of three different values of α and h parameters

$\tilde{E}(M, m, s)$	One dimensional ring		Nanoribbon					
	Ref. [26]		$\alpha = 0.99$		$\alpha = 0.75$		$\alpha = 0.5$	
	$4a_0^*$	$20a_0^*$	$h = 0.001a_0^*$		$h = 0.5a_0^*$		$h = 1.0a_0^*$	
$R(a_0^*)$	$4a_0^*$	$20a_0^*$	$4a_0^*$	$20a_0^*$	$4a_0^*$	$20a_0^*$	$4a_0^*$	$20a_0^*$
$a(0, 0, 0)$	5.18474	22.40328	5.214	22.522	6.044	25.868	7.172	30.827
$b(\pm 1, 1, 1)$	5.68474	22.90328	5.719	23.027	6.700	26.508	8.220	31.630
$c(0, 2, 1)$	7.91615	27.54199	7.916	27.702	9.520	32.331	12.459	39.768
$d(\pm 2, 0, 0)$	7.18474	24.40328	7.234	24.543	8.604	28.428	10.372	34.027
$e(\pm 1, 1, 0)$	8.41615	28.04199	8.469	28.207	10.041	32.971	11.712	40.521
$f(\pm 2, 2, 1)$	9.91615	29.54199	9.989	29.722	12.080	34.891	15.659	42.968
$g(0, 2, 0)$	11.40424	33.36149	11.469	33.569	13.499	39.690	15.014	49.593
$h(\pm 3, 1, 1)$	9.68474	26.90328	9.760	27.068	11.820	31.628	14.620	38.030

4.1.2 Size effects and the influence of the magnetic field

From the curves displayed in Fig. 4.2, it can be seen that ribbon's height and the magnetic field also affect the two-electron energy spectrum. For instance, the little peak in a renormalized energy spectrum as a function of α analyzed in one-dimensional systems (see Fig. 3.5) is also observed in concentric nanoribbons, and according to Fig. 4.2 (a), the greater is the height of the ribbons h the smaller are the peak's height. This behavior is easily explained since for small values of h the two-electron systems undergo a high degree of localization, therefore as α tends to one, the energy peak on the states g, k and n becomes more visible as a consequence of the increment of the electrostatic potential energy.

A clear evidence that the appearing peak is an effect due to geometrical changes arises when the system is in presence of a magnetic field. In Fig. 4.2 (b) is displayed the same energy spectrum for several values of dimensionless magnetic field strength $\gamma(0.0, 0.1, 0.2)$ for a fixed value of $h = 0.0001a_0^*$. Using the first γ value from the set, the curve is identical to the plotted in Fig. 4.2 (a), but as the magnetic field strength is increased the spectrum is risen as a consequence of the additional confinement given by the presence of the field. Nevertheless,

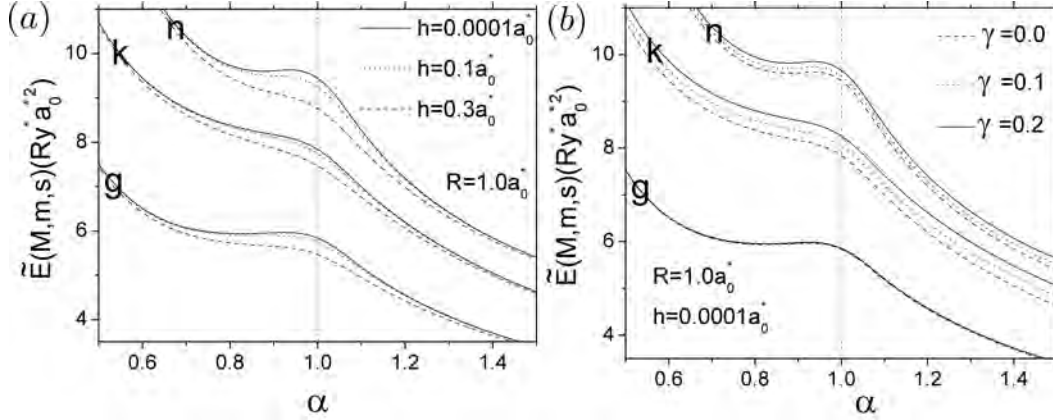


Figure 4.2: renormalized energy for some low-lying states as a function of α parameter. An effect is noticeable as the ribbon's height is varied (a). The presence of magnetic field does not modify the peak morphology near α but provides an additional confinement.

the morphology of the peak does not change drastically because it is inextricably related to the electron-electron interaction. Furthermore, it can be seen that some states are more sensitive to the presence of the magnetic field, in this case the curves of states k and n show a higher increase as the magnetic field strength is raised in comparison with the deeper state g .

4.1.3 Electron-hole pair with same effective masses and Wigner crystallization

The model studied in this work is very flexible and allows to consider an attractive energy potential by taking particles with charges e and $-e$ similar to an exciton. Instead of the repulsive energy potential given by the Eq. 4.1b, it is considered the attractive Coulomb interaction which becomes equal to $-\hat{V}(|\vec{r}_2 - \vec{r}_1|)R^2$. In order to simplify the analysis it is assumed two particles with the same effective masses. In Fig. 4.3, it is presented the comparison between the electron-hole energy spectrum for some low-lying levels confined in nanoribbons (black square symbols) and the spectrum obtained in [63] for an electron-hole system in concentric nanorings (solid solid lines), as a function of the inner radius at zero magnetic field. Both concentric systems have the same radii ratio $\alpha = 0.99$ and the nanoribbons have a very small height $h = 0.0001 a_0^*$.

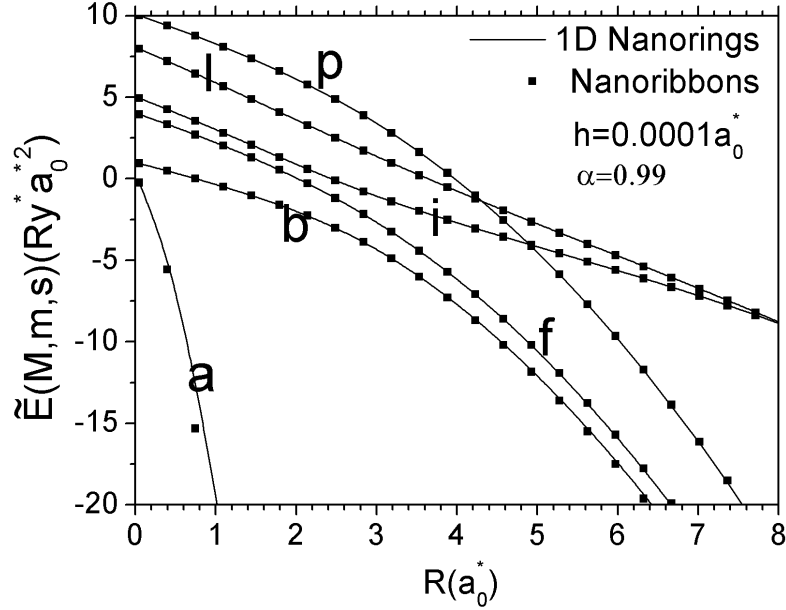


Figure 4.3: Total renormalized energy of an electron-hole system as function of the inner radius in nanoribbons (square symbols) and in one-dimensional nanorings (solid lines). The height of the nanoribbons is small $h = 0.001a_0^*$ and they are very close to each other $\alpha = 0.99$. It is noticeable that the two energy spectra coincides for almost all values of R and all states.

It can be observed the total coincidence between the two sets of results which show the high degree of flexibility of the concentric ribbons model. Furthermore, it can be seen as the inner radius is small the slope of curves change but this slope becomes a constant when the inner radius is large enough. This situation describes a transition between a disordered system, similar to a gas ($\tilde{E}_{Kinetic} > \tilde{U}$) and an ordered system similar to an Wigner ionic crystal ($\tilde{U} > \tilde{E}_{Kinetic}$).

4.2 One and two-particle systems in flat ring-shaped quantum dots

An interesting complex that will be treated in detailed in chapter 6 consists of two electrons released by two on-axis donors into a quantum ring with a very small width. This section is dedicated to the study of one and two-electron systems constrained to move into a two-dimensional flat ring, in presence of two donors which are located at different positions

respect to symmetry center (see Fig. 4.4). Furthermore, it is analyzed and compared these energy spectra.

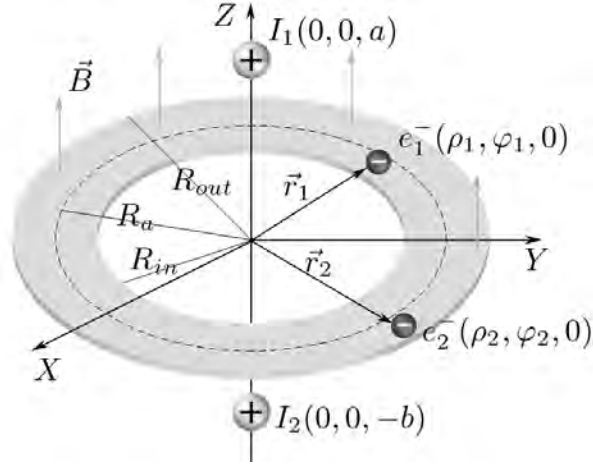


Figure 4.4: Schematic 3D-diagram of a flat ring confining two electrons in presence of two donor impurities

4.2.1 System Hamiltonian

The system Hamiltonian describing the one ($N = 1$) and two-electron ($N = 2$) system in presence of an uniform magnetic field which is oriented along the donor axis and two on-axis donors located at the points $\vec{a} = (0, 0, a)$ and $\vec{b} = (0, 0, -b)$, in the effective-mass approximation can be written in polar cylindrical coordinates $(\rho_k, \varphi_k, 0)$ as follows ¹:

$$\hat{H} = \sum_{k=1}^N \left[-\nabla_k^2 - i\gamma \frac{\partial}{\partial \varphi_k} + \frac{1}{4} \gamma^2 \rho_k^2 + \hat{U}_k(\vec{r}_k) - \frac{2}{|\vec{r}_k - \vec{a}|} - \frac{2}{|\vec{r}_k - \vec{b}|} \right] + \hat{V}(|\vec{r}_2 - \vec{r}_1|) + \hat{V}_{ii} \quad (4.4a)$$

$$\hat{V}(|\vec{r}_2 - \vec{r}_1|) = \frac{2}{|\vec{r}_2 - \vec{r}_1|} \quad (4.4b)$$

$$\hat{V}_{ii} = \frac{2}{|\vec{a} - \vec{b}|} \quad (4.4c)$$

¹The units treated in the section 2.1.1 and the energy labeling shown in Appendix B are also used in this section.

Here the $-\frac{2}{|\vec{r}_k-\vec{a}|}$ and $-\frac{2}{|\vec{r}_k-\vec{b}|}$ terms are the Coulomb interaction energies between electrons and ions and the last two positive terms are the electron-electron ($\hat{V}(|\vec{r}_2-\vec{r}_1|)$) and ion-ion (\hat{V}_{ii}) repulsion respectively. Consequently, following the adiabatic approximation, it is calculated the some low-lying states as a function of the ring radius and the magnetic field strength. The one-electron case is quite simple since $N=1$ and the 4.4b term is null.

4.2.2 Size effects on the energy spectrum

In Figs. 4.6 (a) and (b) are displayed the renormalized energy as a function of the center-line radius for a relative small inter-donor distance equal to $5a_0^*$ for a two-electron and one-electron system, respectively. In both figures is noticeable the renormalized energy sign shift for some states, when the center line radius begins to increase from zero to $15a_0^*$ (Fig. 4.6 (a)) and for the two-first states as R increases from zero to $9a_0^*$.

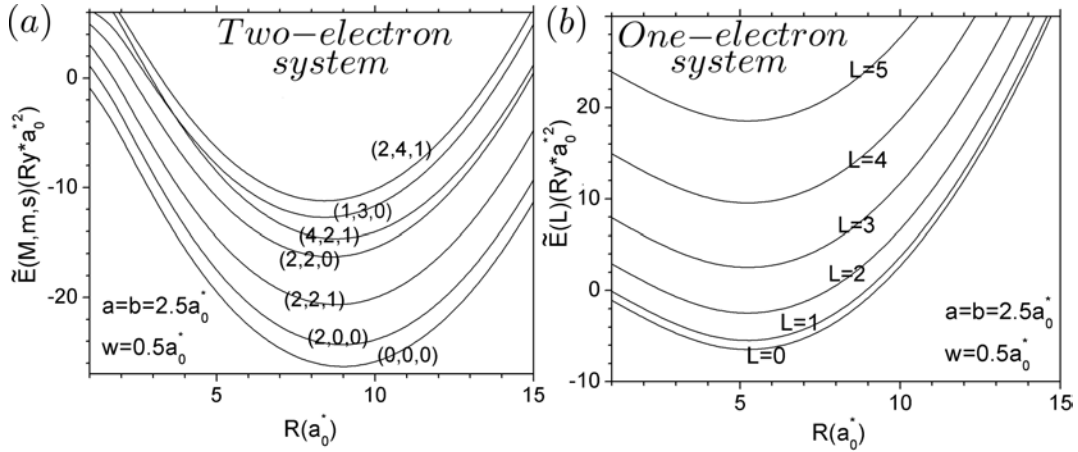


Figure 4.5: Total renormalized energy as function of the center line radius for a two (a) and one-particle system (b) confined in a flat ring in presence of two on-axis impurities. The label L denotes the angular momentum quantum number for the well-known problem of one electron in a single one-dimensional ring [1].

This behavior is explained as an effect of the strong competition between the terms from the Hamiltonian 4.4a, $-\frac{2}{|\vec{r}_k-\vec{a}|}$, $-\frac{2}{|\vec{r}_k-\vec{b}|}$, \hat{V}_{ii} and in the case of the two-electron system the Coulomb term $\hat{V}(|\vec{r}_2-\vec{r}_1|)$. For instance, the states (2, 2, 1) and (2, 2, 0), take positive values

for center line radius lower than $1a_0^*$ and greater than $16a_0^*$ owing to the small values of R the electron-electron and ion-ion repulsion predominates, but as the center-line radius is increased the electron-ion attraction overweights. If the process of increasing R continues, there is a point where the $\hat{V}(|\vec{r}_2 - \vec{r}_1|)$ and \hat{V}_{ii} becomes again predominant.

An important aspect which becomes evident from the two-electron spectrum is that for values of R between zero and $15a_0^*$ the electrons-ions attraction is more noticeable than the electron-ions attraction in the one-electron problem, since in Fig.4.6 (a) for almost all states the energy takes negative values in contrast with the positive values for the one-electron system where the ion-ion repulsion predominates Fig.4.6 (b).

4.2.3 Aharonov-Bohm effect in two-dimensional systems

In Figs.4.6 (a), (b) and (c) are displayed the renormalized energy for a two and one-electron system in a single flat ring, and a two-electron system in concentric ribbons respectively. As expected, for those systems with circular geometry and symmetry is possible to observe the Aharonov-Bohm effect.

The period of the oscillations for all systems can be modified by varying the center-line radius or the inner radius in the case of concentric ribbons. The explicit expressions for the period of a one and two-electron system, can be easily obtained from the eigenenergies of the Hamiltonian 4.4a and are written as follows:

$$T_{one\ e^-} = 2/R^2 \quad (4.5a)$$

$$T_{two\ e^-} = 1/R^2 \quad (4.5b)$$

Nevertheless, the two-electron system in concentric ribbons is more versatile than the other systems since the period of the oscillations is also modifiable by changing the radii ratio or the inner radius which can be calculated from the eigenvalues of the system Hamiltonian 4.1a and is given by:

$$T_{ribbons} = 2/R^2(1 + \alpha^2) \quad (4.6)$$

It is important to mention that with the aim to compare the Aharonov-Bohm oscillations between these systems, the donor impurities positions were located at very distant points from the origin ($a = b = 100a_0^*$), in such a way that the interaction between electrons and

the ions could be assumed negligible. Thus, in this sense, the compared nanostructures confine only negative charge carriers (although as can be seen from Eq.4.5, in this configuration the Aharonov-Bohm oscillations phenomenon is independent of the donors location).

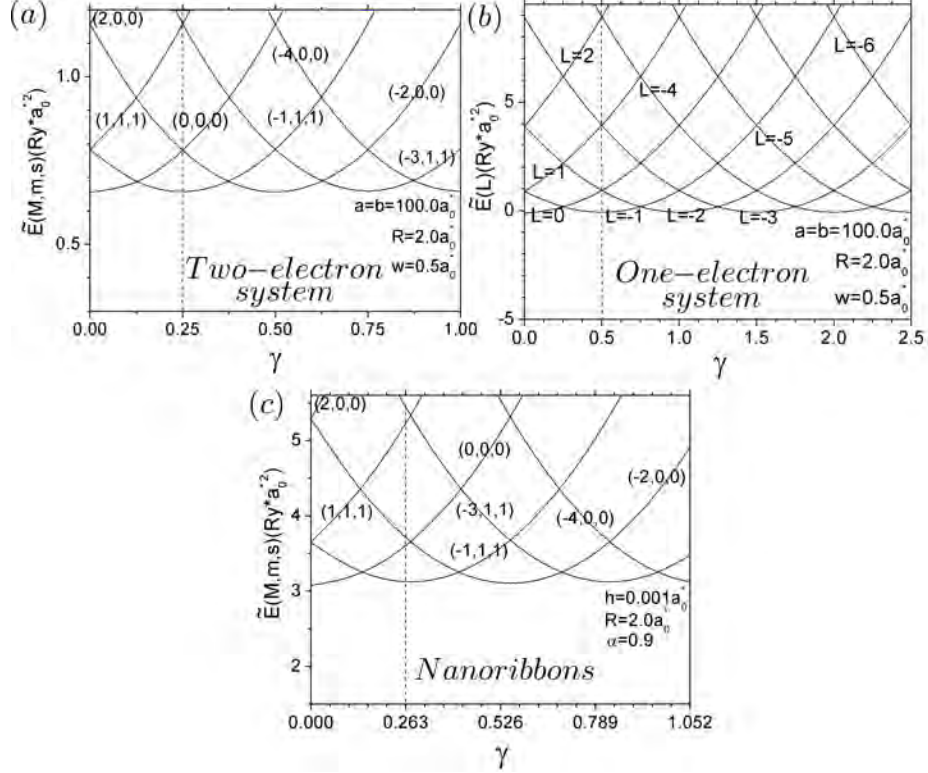


Figure 4.6: Total renormalized energy as function of the magnetic field strength for a two-particle system (a), a one-particle system (b), both in a flat ring, and a two-particle system in two concentric nanoribbons (c). The impurities were moved away to large positions in order to vanish the ion-electron interactions.

From the analysis done above, it is concluded that the separated electrons model offer additional advantages for tailoring the energy spectrum thorough the careful selection and handling of geometrical parameters. In order to study more realistic situations, in the next chapter (5) are analyzed the toroidal quantum rings under the adiabatic approximation method, which will allows to have into account the influence of the cross-section morphology on the energy spectrum.

Chapter 5

Toroidal quantum rings

Very recently, self-assembled double QRs grown in a concentric form [64] or vertically stacked [65] have become a focus of much attention because they present novel properties related to the possibility of controlling the size and the separation between the rings. These facts allow to manipulate the Coulomb interaction between particles and the Aharonov-Bohm [66] oscillations. In spite of the simplest model used to describe ring-like devices and quantum interference effects being based on one-dimensional rings [26, 27, 67], experimental studies [25] and theoretical calculations [68, 32] with only one electron in a single toroidal QR [68] or concentric toroidal QRs [32] have revealed that the energy spectrum is strongly dependent on the shape and size of the QRs. The one-particle energy spectrum has been calculated by using the diagonalization method [68, 32], while the energy structure of neutral and charged donors in a toroidal QR have been analyzed by using the variational method [69] or adiabatic approximation [34]. Bearing in mind that the correlation effects in connection with the QRs have a great influence on the energy structure [68, 32, 69, 34], in this chapter it is proposed a simple method to calculate the spectral properties of two spatially separated electrons, constrained to move in two coaxial and vertically coupled toroidal QRs whose three-dimensional (3D) image is presented in Fig. 5.1. The torus cross-sections to be analyzed are those treated in the section 2.1.2 and also are shown in Fig. 2.1(a).

5.1 System Hamiltonian

The dimensionless Hamiltonian for this two-electron system can be written in cylindrical coordinates as follows:

$$\hat{H} = \sum_{k=1}^2 \left[-\nabla_k^2 - i\gamma \frac{\partial}{\partial \varphi_k} + \frac{1}{4} \gamma^2 \rho_k^2 + \hat{U}_k(\vec{r}_k) \right] + \hat{V}(|\vec{r}_2 - \vec{r}_1|) \quad (5.1a)$$

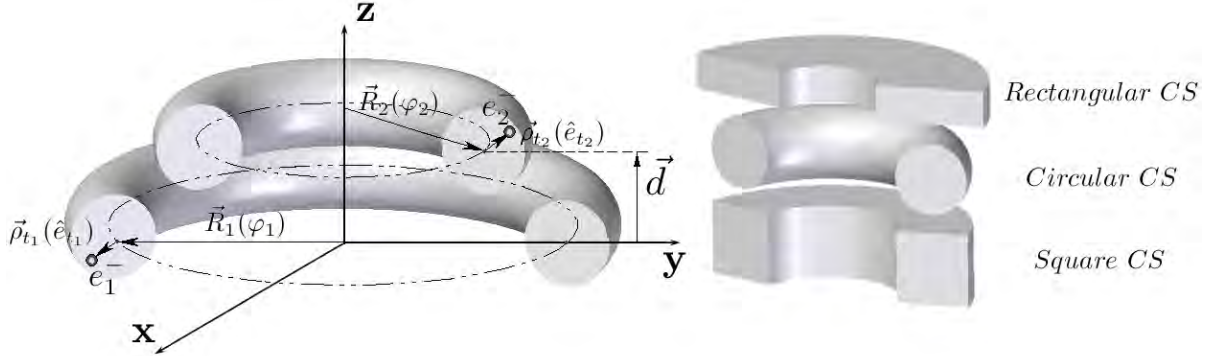


Figure 5.1: Schematic 3D diagram of two electrons in vertically coupled toroidal quantum rings with rectangular, circular and square cross-sections

$$\hat{V}(|\vec{r}_2 - \vec{r}_1|) = \frac{2}{\sqrt{\rho_1^2 + \rho_2^2 - 2\rho_1\rho_2\cos(\varphi_1 - \varphi_2) + (z_1 - z_2)^2}} \quad (5.1b)$$

The vector electron positions described in the section 2.1.2, the energy labeling notation shown in Appendix B and the units treated in the section 2.1.1, are used in this model. In order to find the eigenvalues of the Hamiltonian 5.1, it is supposed that the torus CS is very narrow ($R_k \gg R_t$), allowing to decouple the fast transverse electron motion from the slow rotation motion around the z-axis by using the adiabatic procedure [34]. The low-lying energy levels in this approximation can be found from the following rescaled effective Hamiltonian:

$$\tilde{H} = R^2 \hat{H} = -\left(\frac{\partial^2}{\partial \varphi_1^2} + \frac{1}{\alpha^2} \frac{\partial^2}{\partial \varphi_2^2}\right) - i\gamma \left(\frac{\partial}{\partial \varphi_1} + \frac{\partial}{\partial \varphi_2}\right) + \frac{\gamma^2 R^2}{4} \langle \rho_1^2 + \rho_2^2 \rangle + \bar{V}_{eff}(\varphi_1 - \varphi_2) + E_0 \quad (5.2a)$$

$$\bar{V}_{eff}(\varphi_1 - \varphi_2) = \left\langle f_0^{(1)} f_0^{(2)} \left| R^2 \hat{V}(|\vec{r}_2 - \vec{r}_1|) \right| f_0^{(1)} f_0^{(2)} \right\rangle \quad (5.2b)$$

$$\langle \rho_k^2 \rangle = \left\langle f_0^{(1)} f_0^{(2)} \left| \rho_k^2 \right| f_0^{(1)} f_0^{(2)} \right\rangle \quad (5.2c)$$

Where $f_0^{(k)} = f_0(\rho_{t_k})$ and E_0 are the exact wave function and the corresponding energy in an infinite barrier two-dimensional quantum well related to the electron motion along the cross-section. The eigenvalues of the Hamiltonian 5.2 $\tilde{E} = ER^2$ (with E being the eigenenergies of

\hat{H}) can be found by using the centre-of-mass and relative coordinates. In these coordinates, the Hamiltonian 5.2 can be rewritten as $\tilde{H} = \tilde{H}_\theta + \tilde{H}_\varphi$, where \tilde{H}_θ and \tilde{H}_φ are, respectively, the centre-of-mass and relative terms. The exact eigenvalues $\tilde{E}_\theta(M)$ of the operator \tilde{H}_θ are equal to $M^2/(\alpha^2 + 1) + MR^2\gamma + \frac{1}{4}\gamma^2 R^2 \langle \rho_1^2 + \rho_2^2 \rangle + E_0$, while the eigenvalues of the operator \tilde{H}_φ labeled as $\tilde{E}_\varphi(m, s)$ are determined by numerically solving the eigenvalue problem:

$$\tilde{H}_\varphi \psi_{m,s}(\varphi) = \left[-\left(\frac{1}{\alpha^2}\right) \frac{\partial^2}{\partial \varphi^2} + \tilde{V}_{eff}(\varphi) \right] \psi_{m,s} = \tilde{E}_\varphi(m, s) \psi_{m,s} \quad (5.3)$$

The comparison between the obtained numerical results and the exact solutions previously reported for the limiting cases [26, 27] in a very small CS ($R_t \rightarrow 0$) are presented in Table 5.1. A glance over these data shows that the greater the centre-line radius is the smaller the difference is between the results reported in [26, 27] and the results obtained in the present work. For instance, these energy differences are smaller than $10^{-4} Ry^* a_0^{*2}$ when the centre-line radius is greater than $4a_0^*$. In this sense, these results can be assumed as an indirect proof of the accuracy of the implemented numerical procedure.

Table 5.1: Comparison between the two-electron energies $\tilde{E}(M, m, s)$ obtained in this work for the limiting case ($R_t \rightarrow 0$, $\alpha \rightarrow 1$) (shaded columns) with those previously reported in [26, 27]. For comparison purposes with [27], values of $\alpha = 1$ and $d = 1a_0^*$ were used.

	$R = 1a_0^*$				$R = 4a_0^*$				$R = 20a_0^*$			
	Ref[26]	TQRs	Ref[27]	TQRs	Ref[26]	TQRs	Ref[27]	TQRs	Ref[26]	TQRs	Ref[27]	TQRs
$\tilde{E}(0, 0, 0)$	1.728	1.691	1.226	1.237	5.185	5.184	5.129	5.129	22.403	22.403	22.396	22.396
$\tilde{E}(\pm 1, 1, 1)$	2.232	2.232	2.027	2.027	5.685	5.685	5.634	5.634	22.903	22.903	22.896	22.896
$\tilde{E}(0, 2, 1)$	3.617	3.617	3.204	3.204	7.916	7.916	7.807	7.807	27.542	27.542	27.531	27.531
$\tilde{E}(\pm 2, 0, 0)$	3.728	3.691	3.226	3.237	7.185	7.184	7.128	7.129	24.403	24.403	24.396	24.396

5.2 Two-electron eigenfunctions and probability densities

In the section 2.2 was presented some details of the adiabatic approximation method which was used in order to obtain the two-particle eigenfunction given by the Eq. 2.21 with eigenvalues 2.21b. Owing to the fact that the two-particle wave function is six-dimensional

and with the purpose of making a qualitative description of the the system, it is projected onto some proper planes as shown in Figs. 5.2, where it was assumed that the two electrons are in very narrow and close TQRs at zero magnetic field ($\alpha = 0.99$, $d = 0.01a_0^*$, $\gamma = 0$).

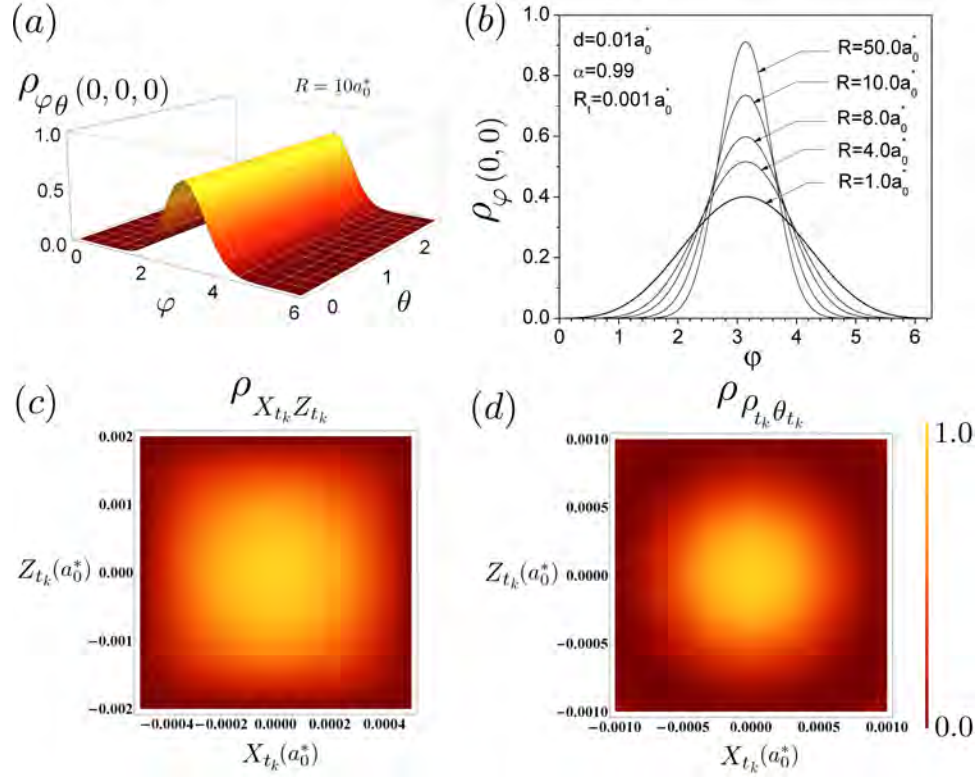


Figure 5.2: Two-dimensional probability density as a function of the centre-of-mass and relative coordinates for a double-ring system with circular CS (a). Probability densities for a TQRs system with circular CS of radius $R_t = 0.001a_0^*$ as a function of φ . Different values of the parameter R were used in order to observe qualitatively a Wigner transition as R is increased (b). Two-dimensional probability densities related to the rapid motion along of a rectangular CS (c) and a circular CS (d). The rectangular CS has dimensions $w = 0.001a_0^*$ and $l = 0.004a_0^*$, while the circular one has a radius equal to $R_t = 0.001a_0^*$.

For example in Fig. 5.2(a), it is plotted the probability density $\rho_{\varphi\theta}(M, m, s)$ for the ground state $(0, 0, 0)$ as a function of φ and θ coordinates. From there, it can be seen that the probability density remains constant for any value of θ , therefore it is equiprobable to find the

center-of-mass of the system anywhere. On the other hand, the probability density takes the maximum value as the relative coordinate is equal to π , thus in this situation, the particles are located diametrically opposed. This fact is observed for different centre-line radii in the Fig. 5.2(b), in which it is plotted the probability density $\rho_\varphi(m, s)$ only as a function of the relative coordinate in the ground state. An interesting phenomenon occurs as the center-line radius increases, giving rise to an simultaneous increment of the maximum of the probability density. This is an additional evidence of the fact that increasing R , the system exhibit a tendency to be more ordered similar to a rigid rotor (Wigner transition).

In Figs. 5.2(c) and (d) are shown the projections of the six-dimensional probability densities onto the planes $X_{t_k} - Z_{t_k}$ and $\rho_{t_k} - \theta_{t_k}$ for the particular cases of two TQRs with rectangular (Fig. 5.2 (c)) and circular (Fig. 5.2 (d)) cross-sections, respectively. These probability densities are related to the fast motion along these cross-sections described by any of the two particles ($k = 1$ or 2) located at the upper or lower ring (the graphical representation of the probability densities of both particles are very similar). From these figures, it is possible to observe that the maximum of the probability densities are located at the center of the potential wells, and tend to zero on the borders as expected. This situation is reasonable since it was assumed that the particles are under a hard-wall confinement regime [48, 37, 38].

5.3 Electron-electron correlation and its influence on the Wigner Crystallization

In Figs. 5.3, the effects of torus CS size and morphology on the two-electron energy are analyzed by considering two different CS sections, circular and square (Fig. 5.3(a)), and three different values of the side h of the square CS (Fig. 5.3(b)). In Fig. 5.3(a), it can be seen that the energy values for electrons in a torus with square CS are always greater than those in a torus with circular CS. This sensitivity of the energy with the CS morphology is a consequence of the greater depth and width of the renormalized effective potential in a torus with circular CS than in the square one, which can be appreciated from the inset of Fig. 5.3(a). In Fig. 5.3(b) the two-electron low-lying state energies are presented as a function of the centre-line radius for two identical tori with square CS and sides $h : 0.001\pi^{1/2}a_0^*$ (solid line) $0.2\pi^{1/2}a_0^*$ (dotted line), $0.3\pi^{1/2}a_0^*$ and (dashed line). The inter-ring distance was taken equal to $d = h + 0.1a_0^*$. Although the torus CS is really small, it can be observed that the greater the CS the smaller the energy values are, which shows that the energy is really sensitive to the CS size variation. Additionally, when R_t and d tend to zero, the low-lying energy states consistently tend to the exact values corresponding to the black square symbols.

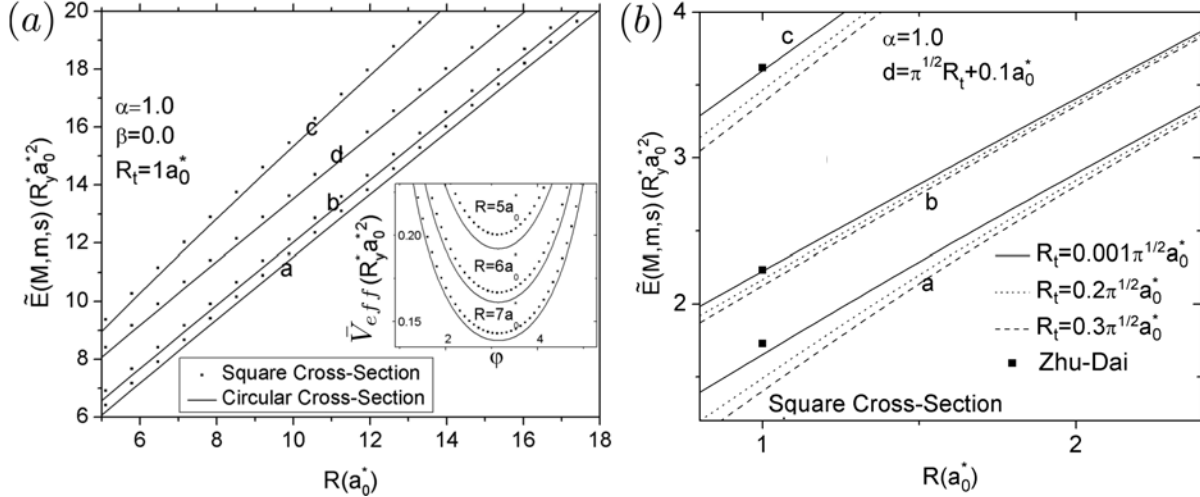


Figure 5.3: Energies $\tilde{E}(M, m, s)$ as a function of the centre-line radius for two different shapes of the torus cross-sections: circular (solid line) and square (dot symbols) (a) and three different values of the square cross-section side (b).

The low-lying energy states as a function of the centre-line ring radius for electrons in a square CS torus are shown in Figs. 5.4. Two different separations between rings were considered: $d = 5a_0^*$ ($\alpha = 0.85$, Fig. 5.4(a) and $\alpha = 0.3$, Fig. 5.4(b)) and $d = 0$ ($\alpha = 0.85$, Fig. 5.4(c)). The remarkable evolution of these energy levels may be explained by taking into account that the renormalized kinetic energies are independent of R , while the renormalized potential is proportional to R . For this reason, as R is small, the slopes of the curves are permanently changing and crossing, which is an indicator of the existence of a strongly disordered system. But as R increases, the slope of the curves become constant, which is associated with a strongly correlated system similar to a Wigner crystal. Additionally, it can be observed that the greater α is, or the smaller d is, then the crossover between energy levels takes place for much smaller values of R .

From Figs. 5.3(a), 5.3(a) and 5.4 it is concluded that the particle-particle interaction plays an important role on the properties of the system. In this particular case, by varying some geometrical parameters related to the size and shape of the TQRs system, it is possible to induce a transition from a disordered to an ordered system (Wigner crystallization) which is clearly noticeable from the evolution of energy spectrum and the probability density with the centre-line radius, the center-lines radii ratio and the inter-ring distance.

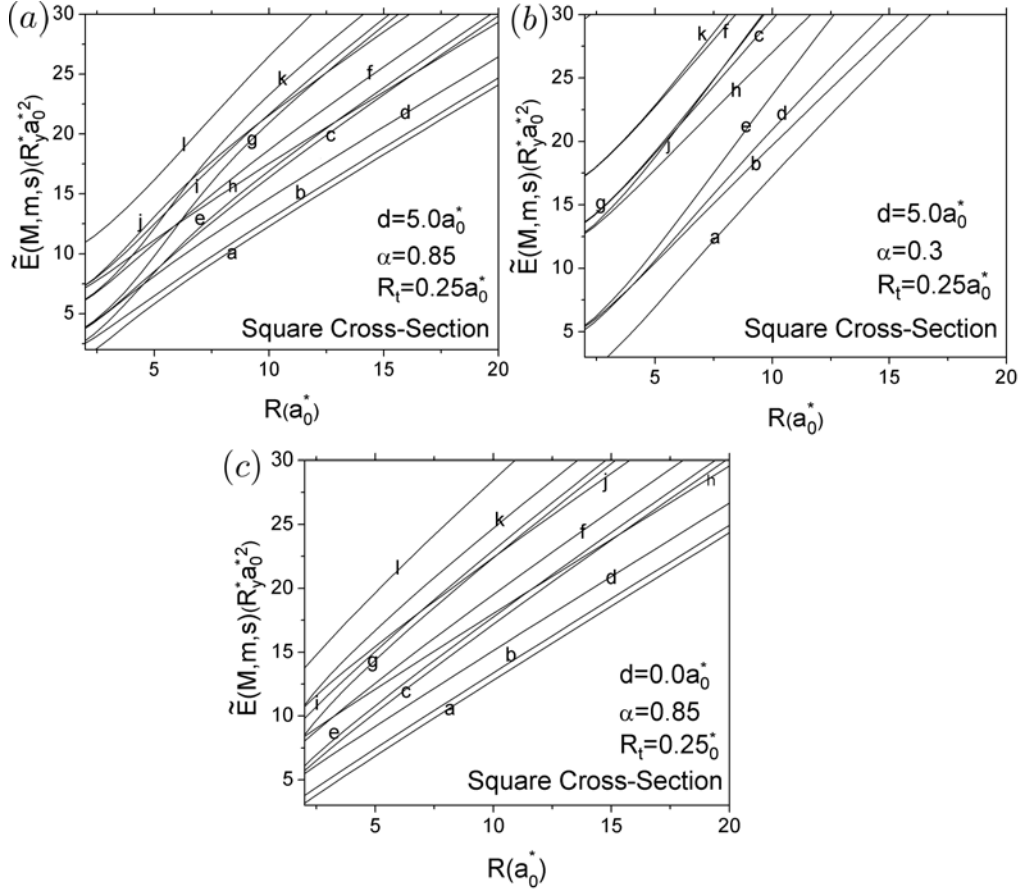


Figure 5.4: Energies of the first low-lying states as a function of the centre-line radius for tori with square cross-section.

5.4 Aharonov-Bohm effect in vertically coupled toroidal quantum rings

Finally, the total renormalized energy as a function of the renormalized magnetic field strength γR^2 for electrons in concentric tori with circular CS with $\alpha = 1$ and $\alpha = 1.5$ is shown in Fig. 5.5(a) and (b), respectively. From these figures it can be concluded that the smaller α is the greater are the energy values and the AB oscillation period T . All curves with $M < 0$ take minima for values $\gamma = 2|M|/1 + \alpha^2$, making the AB oscillation period for a narrow nanoring becomes approximately equal to $2/(1 + \alpha^2)$ (see chapter 3).

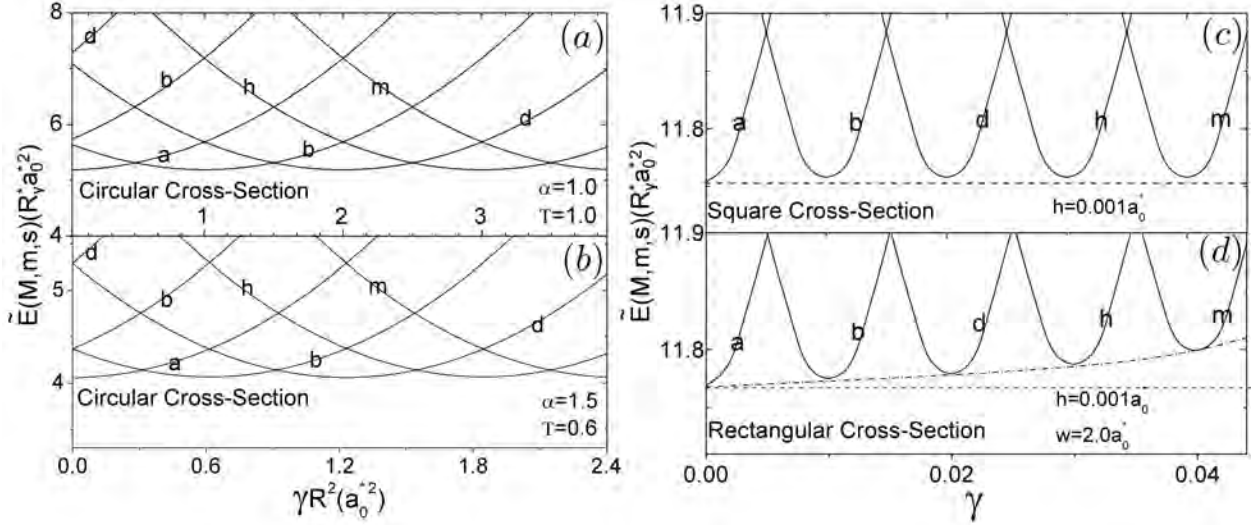


Figure 5.5: Energies $\tilde{E}(M, m, s)$ as a function of the renormalized magnetic field strength for tori with circular CS (a,b). Energies $\tilde{E}(M, m, s)$ as a function of the magnetic field strength for tori with square CS (c) and rectangular CS (d). Values of $R = 4a_0^*$, $R_t = 0.001a_0^*$, and $\beta = 0.0$ were used in (a, b), and $R = 10a_0^*$, $\alpha = 1$, and $\beta = 0.0$ were used in (c, d).

The total renormalized energy as a function of the magnetic field strength for electrons in a single torus with a square and a rectangular CS is displayed in Fig. 5.5(c) and (d), respectively. Although the AB oscillations appear to be sinusoidal, such as shown in Fig. 5.5(c), they move away from this behavior when the rings are not very narrow, as can be seen in Fig. 5.5(d). This is due to the variation of the ring width $w = R_{outer} - R_{inner}$ defined as the difference between the outer and inner radii, which yields a distortion of the AB oscillation period. Therefore, a quenching of the AB oscillations is expected to appear for large values of the QR thickness, but this effect is impossible to obtain from this model because the conditions under which using the adiabatic procedure are not satisfied.

Chapter 6

Artificial Molecules

In recent years there has been reported the fabrication of self-assembled quantum rings with very small thickness to outer-radius aspect ratio [25]. This finding has attracted a great deal of theoretical attention in the study of the few-particle energy spectrum confined in such QRs. The exact series solution for the two-electron problem in the extreme adiabatic limit has been analyzed as the width and the height of the QR are negligible; see [26, 27]. In order to take into account the effect of the finite QR thickness, the adiabatic approximation technique has been recently used [70] with the purpose of calculating the lowest-energy states of an artificial negative hydrogen ion in a narrow toroidal-shape ring. In this chapter it is used a similar approach in order to study the low-lying energy states of an artificial hydrogen molecule H_2 which consists of two on-axis ionized donors located symmetrically respect to the origin at the points $\vec{a} = (0, 0, \zeta/2)$ and $\vec{b} = (0, 0, -\zeta/2)$, being $\zeta = 2|\vec{a}| = 2|\vec{b}|$ the donor-donor distance, and two electrons released inside of a narrow toroidal ring. The QR is generated by the revolution around the Z-axis of a small circle of radius R_t centred at the distance R ($R \gg R_t$) from the symmetry axis. A schematic three-dimensional (3D) image of the model is shown in Fig. 6.1.

6.1 System Hamiltonian

The dimensionless Hamiltonian describing the artificial hydrogen molecule in a toroidal QR under the presence of an external and homogeneous magnetic field $\vec{B} = B\hat{k}$ can be written in cylindrical coordinates (ρ, φ, z) in the form

$$\hat{H} = \sum_{k=1}^2 \left[-\nabla_k^2 - i\gamma \frac{\partial}{\partial \varphi_k} + \frac{1}{4} \gamma^2 \rho_k^2 + \hat{U}_k(\vec{r}_k) - \frac{2}{|\vec{r}_k - \vec{a}|} - \frac{2}{|\vec{r}_k - \vec{b}|} \right] + \hat{V}(|\vec{r}_2 - \vec{r}_1|) + \hat{V}_{ii} \quad (6.1a)$$

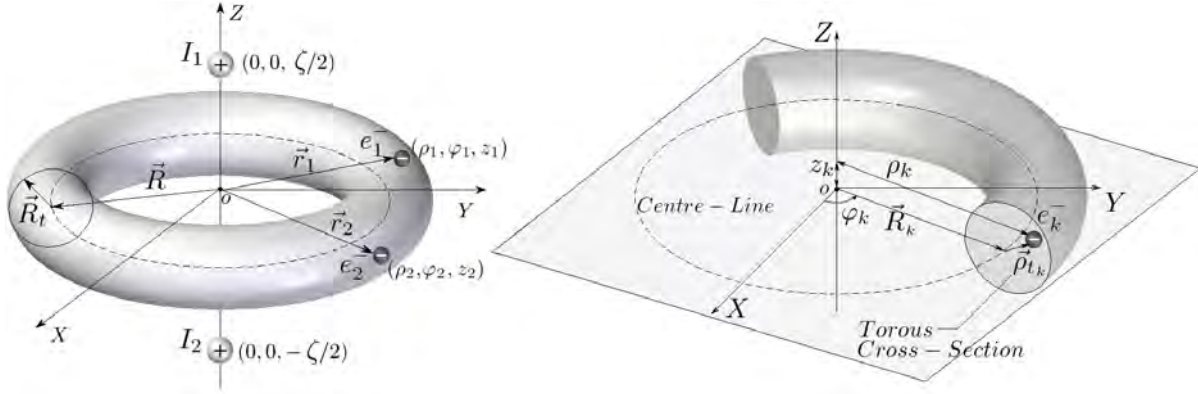


Figure 6.1: Three-dimensional model image of the artificial hydrogen molecule.

$$\hat{V}(|\vec{r}_2 - \vec{r}_1|) = \frac{2}{|\vec{r}_2 - \vec{r}_1|} \quad (6.1b)$$

$$\hat{V}_{ii} = \frac{2}{|\vec{a} - \vec{b}|} \quad (6.1c)$$

The vector electron positions described in the section 2.1.2, the energy labeling notation shown in Appendix B and the units treated in the section 2.1.1, are used in this model. The terms $-\frac{2}{|\vec{r}_k - \vec{a}|}$ and $-\frac{2}{|\vec{r}_k - \vec{b}|}$ in the Hamiltonian 6.1 are the Coulomb interaction energies between electrons and ions, and the last two positive terms are the electron-electron $\hat{V}(|\vec{r}_2 - \vec{r}_1|)$ and ion-ion \hat{V}_{ii} repulsion, respectively. It is important to notice that in this model, the magnitude for both vector \vec{R}_k are equal to R , this is, ($|\vec{R}_1| = |\vec{R}_2| = R$) (see Fig. 6.1). Consequently by considering a narrow toroidal QR ($R \gg R_t$), it is possible to use the well-known adiabatic procedure (see section 2.2). First, it is necessary to find out the ground-state wave function $f_0^k(\vec{\rho}_{t_k})$ ($k = 1, 2$) and its corresponding energy E_0 for each electron in an infinite two-dimensional circular quantum well of radius R_t . Second, in order to obtain all the low lying-energy levels, it is necessary to solve the wave equation with the effective Hamiltonian given by

$$\hat{H}_a = -\frac{1}{R^2} \left(\frac{\partial^2}{\partial \varphi_1^2} + \frac{\partial^2}{\partial \varphi_2^2} \right) - i\gamma \left(\frac{\partial}{\partial \varphi_1} + \frac{\partial}{\partial \varphi_2} \right) + \frac{1}{4} \gamma^2 R^2 \langle \rho_1^2 + \rho_2^2 \rangle + 2E_0 + \frac{2}{R} + \bar{V}_{eff}(\varphi_1 - \varphi_2) + \bar{V}_{ei} \quad (6.2a)$$

$$\bar{V}_{eff}(\varphi) = \left\langle f_0^1 f_0^2 \left| \frac{2}{\sqrt{|\vec{r}_{t_1} - \vec{r}_{t_2}|^2 + 4R^2 \sin^2(\varphi/2)}} \right| f_0^1 f_0^2 \right\rangle \quad (6.2b)$$

$$\bar{V}_{ei} = -2 \left\langle f_0^k \left| \hat{V}_+(\rho_{t_k}, \varphi_{t_k}) + \hat{V}_-(\rho_{t_k}, \varphi_{t_k}) \right| f_0^k \right\rangle \quad k = 1, 2 \quad (6.2c)$$

$$\hat{V}_\pm(\rho_{t_k}, \varphi_{t_k}) = \frac{1}{\sqrt{(\rho_{t_k} \sin \varphi_{t_k} \pm \zeta/2)^2 + (R + \rho_{t_k} \cos(\varphi_{t_k}))^2}} \quad (6.2d)$$

$$\langle \rho_k^2 \rangle = \langle f_0^k | \rho_k^2 | f_0^k \rangle \quad k = 1, 2 \quad (6.2e)$$

As the effective potential in the Hamiltonian 6.2a depends only on the difference of the angular coordinates, the corresponding wave equation can be separated by using the centre of mass and relative coordinates, allowing to rewrite the two-particle Hamiltonian as the sum of the centre of mass \hat{H}_θ and relative \hat{H}_φ terms:

$$\hat{H} = \hat{H}_\theta + \hat{H}_\varphi + 2E_0 + \bar{V}_{ei} + \frac{2}{\zeta} \quad (6.3a)$$

$$\hat{H}_\theta = -\frac{1}{2R^2} \frac{\partial^2}{\partial \theta^2} - i\gamma \frac{\partial}{\partial \theta} + \frac{1}{4} \gamma^2 R^2 \langle \rho_1^2 + \rho_2^2 \rangle \quad (6.3b)$$

$$\hat{H}_\varphi = -\frac{2}{R^2} \frac{\partial^2}{\partial \varphi^2} + \bar{V}_{eff}(\varphi) \quad (6.3c)$$

And their eigensolutions are given by:

$$\Psi(\varphi_1, \varphi_2) = e^{iM\theta} \psi_{m,s}; \quad M, m = 0, \pm 1, \pm 2, \dots; \quad s = 0, 1 \quad (6.4)$$

Here, the functions $e^{iM\theta}$ in 6.4 are the solutions of the wave equation with Hamiltonian \hat{H}_θ and their corresponding eigenvalues are $E_\theta(M) = \frac{M^2}{2R^2} + M\gamma + \frac{1}{4} \gamma^2 R^2 \langle \rho_1^2 + \rho_2^2 \rangle$. The remaining factor $\psi_{m,s}(\varphi)$ in 6.4 is the solution of the following one-dimensional wave equation corresponding to the relative angular motion and satisfy the periodic boundary conditions given by 6.5b

$$-\frac{2}{R^2} \frac{\partial^2 \psi_{m,s}(\varphi)}{\partial \varphi^2} + \bar{V}_{eff}(\varphi) \psi_{m,s}(\varphi) = E_\varphi(m, s) \psi_{m,s}(\varphi) \quad (6.5a)$$

$$\psi_{m,s}(-\varphi) = (-1)^s \psi_{m,s}(\varphi); \quad \psi_{m,s}(\varphi) (-1)^M = \psi_{m,s}(\varphi \pm 2\pi) \quad (6.5b)$$

The total energy levels $E(M, m, s) = E_\theta(M) + E_\varphi(m, s) + \bar{V}_{ei} + \frac{2}{\zeta}$ are referred to the non-interacting two-electron ground-state energy in a circular infinite quantum well, and therefore the term $2E_0$ has been neglected in the total energy $E(M, m, s)$.

6.2 Size and impurities location effects on the molecular energy spectrum

The comparison between the numerical calculations for the renormalized energies, $\tilde{E} = R^2 E(M, m, s)$ obtained in this work, with those from [26, 27] for two electrons in a one-dimensional QR are presented in Table 6.1. As the separation between ions increases between $0.1a_0^*$ and $100a_0^*$ and the toroidal radius cross-section tends to zero, the contributions of the electron-ion and ion-ion interactions become very small, and therefore the artificial hydrogen molecule energies in Table 6.1 successively tend to the renormalized energy values for two electrons constrained to move in a one-dimensional quantum ring [26, 27]. Such correct tendency of the obtained results with the proposed model can be considered as an indirect proof of the accuracy and acceptability of the numerical procedure.

Table 6.1: Some of the renormalized low-lying energy levels $\tilde{E} = R^2 E(M, m, s)$ of the artificial hydrogen molecule for two different radii of the centre-line R and four different separations ζ between ions. Renormalized energies and distances are given in units of $Ry^* a_0^{*2}$ and a_0^* , respectively. A value of $R_t = 0.001a_0^*$ was used for comparison purposes with [26].

(M, m, s)	$R = 1a_0^*$					$R = 4a_0^*$				
	$\tilde{E}(M, m, s)$	Artificial molecule				$\tilde{E}(M, m, s)$	Artificial molecule			
	Ref. [26]	$\zeta = 100$	$\zeta = 20$	$\zeta = 1$	$\zeta = 0.1$	Ref. [26]	$\zeta = 100$	$\zeta = 2$	$\zeta = 1$	$\zeta = 0.1$
(0, 0, 0)	1.72	1.65	-0.79	-3.44	13.72	5.18	4.96	-9.11	5.43	293.19
(1, 1, 1)	2.23	2.16	-0.31	-2.92	14.24	5.68	5.46	-8.61	5.93	293.68
(0, 2, 1)	3.61	3.53	1.09	-1.54	15.63	7.92	7.69	-6.38	8.16	295.91
(2, 0, 0)	3.72	3.66	1.19	-1.44	15.72	7.18	6.96	-7.11	7.43	295.18

In Fig. 6.2, it is displayed the results of calculation of the artificial hydrogen molecule ground-state energy at zero magnetic field as a function of the separation between ions for different values of the torus thicknesses 6.2(a) and the torus radii 6.2(b). From these curves we can observe the similarity between the potential curves of the actual (dotted line from [71]) and the artificial hydrogen molecules (solid lines). These results illustrate a wide range

of possibilities to modify the equilibrium distance and the barrier height of the artificial molecule by varying the ring thickness or the ring centre-line radius.

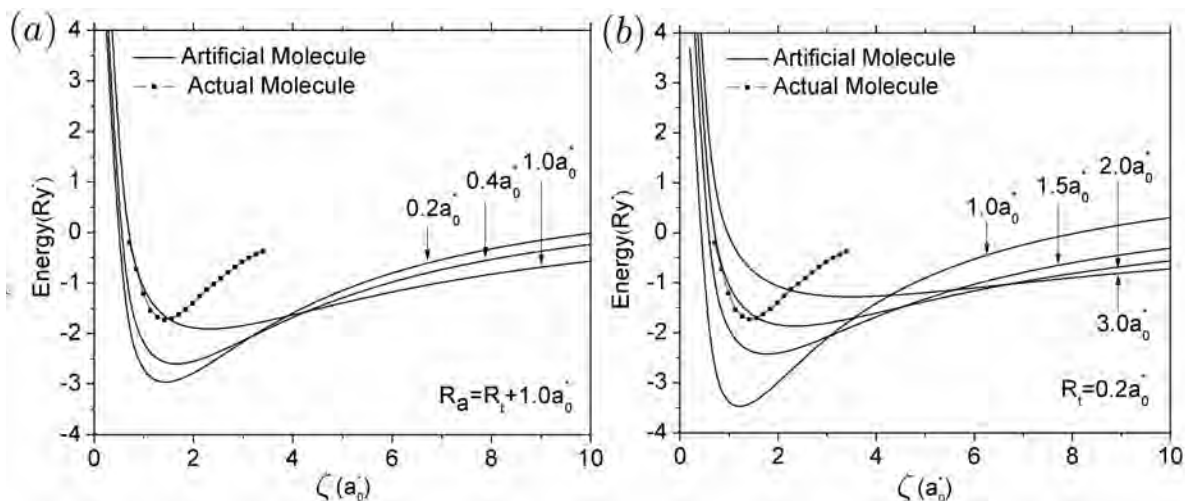


Figure 6.2: Ground-state energy of an artificial hydrogen molecule as a function of the distance between ions for different ring thicknesses (a) and ring radii (b). The dotted line corresponds to the potential curve of the actual hydrogen molecule.

In Fig. 6.2(a), it can be seen that the potential curves for different ring thicknesses have an almost common intersection point in which the separation between ions is about $4a_0^*$ and the molecule energy is about $-1.7Ry^*$. This peculiarity can be related to the transformation that the electron arrangement undergoes as the separation between ions becomes greater than $4a_0^*$. For small separations between ions, the attraction outweighs the repulsion, and therefore the electrons are more probably located close to the torus interior frontier, i.e., the electrons are nearer to the ions; but when the inter-ion separation becomes greater than $4a_0^*$, the electrons are displaced toward the exterior torus frontier and the order of the energy levels is inverted.

In Fig. 6.2(b), it can be clearly observed the crossovers of the potential curves at different points and the inversion the order of the energy levels. This fact is a consequence of the interplay between the interparticle repulsion and attraction since if the separation between ions is very small the largest contribution to the total energy is given by the ion-ion repulsion followed by the electron-ion attraction, while the smallest one is given by the electron-electron repulsion. As the positive contribution of the ion-ion interaction defines the sign of the total energy and it is the same for all ring radii, the order of the levels depends only on the rela-

tive values of the other two interaction types. The absolute values of both the electron-ion interaction and the electron-electron repulsion are larger in rings with smaller radii.

For small separations between ions, the negative energy of the electron-ion attraction can be greater than the positive energy of the electron-electron repulsion, and therefore the total energy of the artificial molecule with smaller ring radius is lower. Conversely, for large distances between ions, the repulsion is greater than the attraction, and the structures with greater ring radius have lower ground-state energies. For this reason, the curves in Fig. 6.2 display intersections and inversion of the order in the ground-state energy levels for structures with different ring radii.

In Fig. 6.3, it is shown similar potential curves corresponding to some of the low-lying energy levels of the artificial hydrogen molecule with ring centre-line radius $R = 1a_0^*$ and ring cross-section radius $R_t = 0.2a_0^*$. It is seen that all potential curves have deep minima with barrier heights greater than $3Ry^*$, and therefore all these states become very stable. In accordance with Fig. 6.3, it can be seen that the molecule ground state is singlet and it is followed by the first triplet state. This behavior is independent of the ion-ion separation.

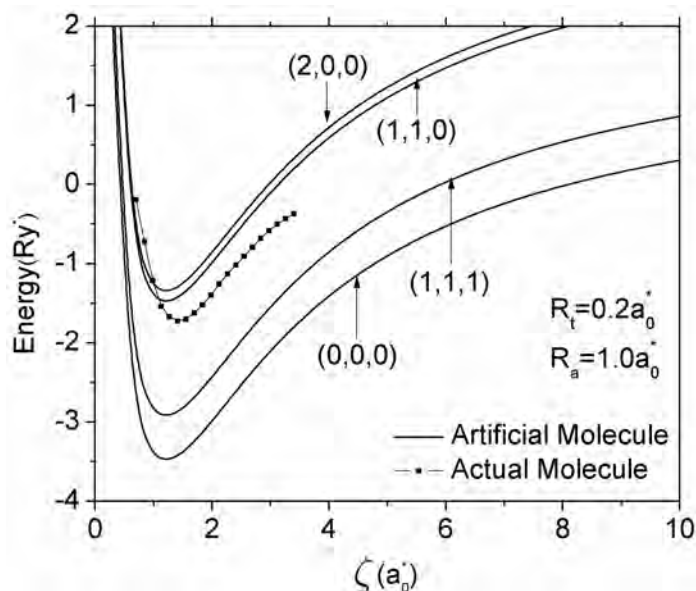


Figure 6.3: Some of the low-lying energy levels of an artificial hydrogen molecule as a function of the distance between ions. The dotted line shows the actual hydrogen molecule ground state.

6.3 Artificial molecule in presence of a uniform magnetic field

Finally, some energy levels $E(M, m, s)$ of the two-electron artificial molecule in toroidal QRs as a function of the renormalized magnetic field (γR_a^2) are shown in Fig. 6.4 for radius of the centre-line $R = 3a_0^*$, radius of circular cross-section $R_t = 0.2a_0^*$ and two different separations between ions: $\zeta = 0.5a_0^*$ (Fig. 6.4(a)) and $\zeta = 5a_0^*$ (Fig. 6.4(b)). In order to understand the remarkable evolution of the energy curves displayed in Fig. 6.4, it must be kept in mind that these curves are the result of the strong competition between two pairs of parameters present in the Hamiltonian 6.1. The first pair corresponds to the repulsive and attractive potential terms and the second pair corresponds to the paramagnetic and diamagnetic terms. The first pair of parameters allows to explain the reason why the energy takes positive or negative values. For instance, if the separation between ions is smaller than $0.5a_0^*$, the contribution of the ion-ion repulsion term is predominant and the total energy takes positive values (Fig. 6.4(a)), but if this separation is greater than $5a_0^*$ then the attractive term becomes more significant and the total energy minima take negative values (Fig. 6.4(b)). The presence of the magnetic field in the second pair of parameters allows to explain two important aspects.

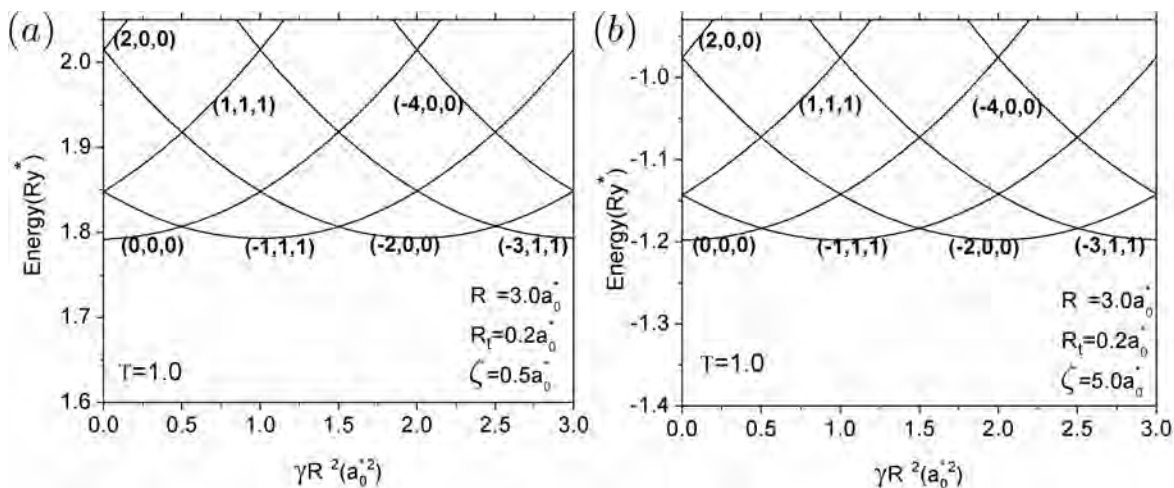


Figure 6.4: The lowest energy levels of an artificial hydrogen molecule as a function of the renormalized magnetic field in a toroidal quantum ring with ion-ion separation $\zeta = 0.5a_0^*$ (a) and $\zeta = 5a_0^*$ (b). The centre-line radius R and the circular cross-section radius R_t are equal to $3a_0^*$ and $0.2a_0^*$, respectively.

On the one hand, since the paramagnetic term varies linearly with the magnetic field and the angular momentum M , this term is responsible for the splitting in the energy levels whose angular momentum M has different signs. For instance, when $M > 0$ all curves are linear at the beginning with positive slope, but when $M < 0$ the slope becomes negative. On the other hand, and according to Fig. 6.4, it can be observed an oscillatory behavior in the molecular complex ground-state energy with period $T = \gamma R^2 = 1$ which remains constant for all values of the centre-line radius when the circular cross-section radius to centre-line radius aspect ratio is very small. This result corresponds to the well-known Aharonov-Bohm effect [72]. In order to understand the behavior of these curves, it is necessary to take into account that, for small values of the magnetic field strength, the paramagnetic term predominates over the diamagnetic term which is quadratic with the magnetic field. Nevertheless, this behavior changes for large values of the magnetic field strength, since the contribution of the diamagnetic term to the total energy becomes more significant than the paramagnetic term, which allows to explain the parabolic shape of all the curves above a given value of the field strength.

Conclusions

The analysis done in this work related to the few-particle systems studied throughout the several chapters, allows to establish some relevant aspects that summarize the results obtained and lead to the following ideas:

- The size of the quantum rings are shown to be fundamental in determining the carrier dynamics inside of these nanostructures. For instance, it is observed a disordered to ordered structural transition (Wigner transition) as the interring instance or the radii ratio is varied, being this effect more noticeable when the ring radii are small. In this sense, the particle-particle interaction plays a significant role on the quantum levels.
- The influence of the cross-section morphology on the tow-particle energy spectrum was demonstrated. This fact is really important since the ring cross-sections considered were really small. In the particular case of GaAs materials, in which the effective Rydberg is equal to $Ry^* = 5.8 \text{ meV}$, the energy difference between different morphologies with the same area are close to 0.1 meV . According to some modern measurement devices [73] such energies can be detected. But when the radii of the rings are too greater in comparison with the cross-section dimensions, the energy discrepancy becomes almost negligible. In this case a one-dimensional or two-dimensional model is a good first approximation to model the system.
- When the studied quantum rings are in presence of an uniform magnetic field, an oscillatory behavior of the system spin-shift related to the ground state occurs as the magnetic field strength is increased (Aharonov-Bohm effect). In the case of one-particle systems the period is modifiable by means of the ring radius and for two-particle systems it is also tailorable thorough the rings (or ribbons) radii ratio. Undoubtedly, this is an interesting phenomenon in the study of equilibrium and transport properties in nanostructures.
- The energy spectrum of quantum rings in presence of donor impurities exhibit an exotic behavior similar to actual molecules. The proposed model of artificial molecules consisting of electrons released by on-axis donors inside of toroidal narrow rings allows to explore a great variety of properties which the artificial molecule has in contrast to the single option given by actual molecules provided by nature. It is shown that the

shapes and positions of the potential curves in the artificial molecule may be tailored essentially by varying the donor positions, the radius and thickness of the ring. In this sense, these systems could be implemented in potential applications such as the case of innovative optoelectronic devices. Consequently, the theoretical calculations realized in this thesis could be useful for this purpose.

- In short, the energy spectrum of the studied nano-systems are strongly dependent on the size and shape of the confining nanostructures, the nature of the external applied fields and the number and type of the confined particles.

Appendix A

Trigonometric Sweep Method

The problems treated in the several chapters, involve at some point in the modeling process the solution of eigenvalue problems related to the dimensionless Schrödinger equation, which can be rewritten in a standard form as follows:

$$-C \frac{\partial^2}{\partial \varphi^2} \Psi(\varphi) + \tilde{V}(\varphi) \Psi(\varphi) = \tilde{E} \Psi(\varphi) \quad (\text{A.1})$$

Where C is a constant characteristic of each system, and the pair of terms \tilde{V} and \tilde{E} are the renormalized¹ potential and energy, respectively. On the other hand, $\Psi(\varphi)$ and \tilde{E} are in that order, the eigenfunctions and eigenvalues associated with the wave differential equation that describes such one-dimensional system.

In the literature [47, 51, 50] are presented diverse numerical methods for solving differential equations, the most representative are the Runge Kutta-method, Shooting Method among others. But solving the second-order differential equation (A.1) involved an additional degree of complexity because its solution depends on the unknown parameter \tilde{E} , thus a further algorithm must be developed. In order to solve this eigenvalue problem it is possible to perform some developed algorithms, as those suggested in [50], but often are not very efficient computationally because they involve solving several times the same second-order differential equation by varying the parameter \tilde{E} until a specific boundary condition is satisfied.

The objective of using trigonometric sweep method is reducing the order of the differential equation and making the process of finding eigenvalues and eigenfunctions more efficiently. This can be achieved if the state of the system is described in a phase-space plane (see Fig.

¹The actual quantities are proportional to the renormalized ones, and they are introduced by a rescaling transformation with the aim of simplifying the computational process.

A.1) by using the Poincaré polar coordinates. The explicit transformation can be written as follows:

$$\Psi(\varphi) = A(\varphi)\cos(\alpha(\varphi)) \quad (\text{A.2a})$$

$$\Psi'(\varphi) = A(\varphi)\sin(\alpha(\varphi)) \quad (\text{A.2b})$$

Here, the wavefunction is written in terms of two quantities, $A(\varphi)$ and $\alpha(\varphi)$, which represent the amplitude and phase, respectively of $\Psi(\varphi)$ on the phase-space plane.

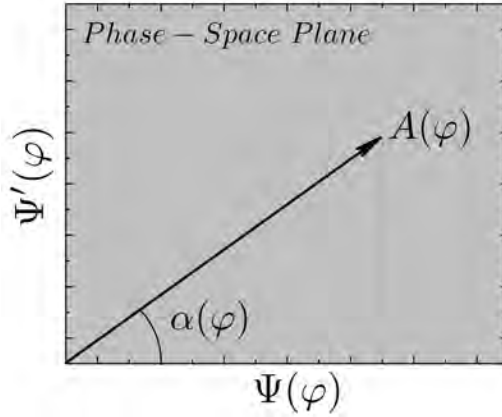


Figure A.1: Phase-space plane. The $A(\varphi)$ and $\alpha(\varphi)$ quantities defined into the transformations A.2 are interpreted as the amplitude and phase of Poincaré curves respectively.

Following with the order-reduction process, it is easy to show that relations (A.1) and (A.2) satisfy the following relations

$$\frac{\Psi''(\varphi)}{\Psi(\varphi)} = \frac{1}{C}(\tilde{V}(\varphi) - \tilde{E}) = \tan^2(\alpha(\varphi)) + \sec^2(\alpha(\varphi))\alpha'(\varphi) \quad (\text{A.3})$$

allowing to obtain a first-order differential equation for the phase function $\alpha(\varphi)$ giving by:

$$\alpha'(\varphi) + \sin^2(\alpha(\varphi)) + \cos^2(\alpha(\varphi))\left(\frac{\tilde{E} - \tilde{V}(\varphi)}{C}\right) = 0 \quad (\text{A.4})$$

Which is solved numerically via Runge-Kutta-Fehlberg Method (RKF45). But for this purpose, an initial condition in order to initiate the algorithm execution is needed. Such initial

condition arises from the physical fact that the $\tilde{V}(\varphi)$ functions in the present work are periodic² and can be interpreted as confinement potentials³.

It is well known from several problems in quantum mechanics⁴ that the single or even states are characterized by a wavefunction with a slope which slowly tends to zero at the frontier points, while the triplet or odd states wavefunctions tends to zero at such points [38, 37]. These conditions can be written, assuming that the potential confinement frontiers are located at $\varphi = 0$ and $\varphi = 2\pi$ as:

$$\Psi'(\varphi = 0) = \Psi'(\varphi = 2\pi) = 0 \quad \text{for singlet states } (s = 0) \quad (\text{A.5a})$$

$$\Psi(\varphi = 0) = \Psi(\varphi = 2\pi) = 0 \quad \text{for triplet states } (s = 1) \quad (\text{A.5b})$$

Where s labels the parity of the state, taking the value of 0 and 1 for singlets and triplets states, respectively. Despite the potential confinement imposes sets physical boundary conditions directly on the wavefunctions, the Poincaré coordinates (A.2) and conditions (A.5) allows us to find an initial condition and a boundary condition for α function, which can be easily obtained and are given by:

<i>initial conditions</i>	<i>boundary conditions</i>	
$\alpha(\varphi = 0) = 0$	$\alpha(\varphi = 2\pi) = -m\pi$	<i>for singlet states</i> ($s = 0$) (A.6a)
$\alpha(\varphi = 0) = \frac{pi}{2}$	$\alpha(\varphi = 2\pi) = -m\pi + \frac{\pi}{2}$	<i>for triplet states</i> ($s = 1$) (A.6b)

Here, m takes values $m = 0, \pm 1, \pm 2, \dots$ and it is called the relative angular quantum number.

The process of solving Eq.(A.4) with boundary conditions (A.6) begins by introducing values of the entry parameters s and \tilde{E} ⁵, then Eq.(A.4) is solved obtaining an $\alpha(\varphi)$ function. As can be noticed, the solution depends on the entry parameters, although the function $\alpha(\varphi)$ explicitly does not. By this reason it is introduced the $v(\varphi, \tilde{E}, s)$ function, which corresponds

²In all cases treated in this document, the geometry of TQRs systems impose a periodicity of 2π on the potential. Thus, odd and even solutions of the wavefunction are expected.

³This fact entails a particular behavior on the wavefunction at the frontier points.

⁴Such the particular case of infinite barrier quantum well

⁵For practical purposes the selected initial value of \tilde{E} must coincide with the confinement potential minima.

to the solution of Eq.(A.4) for a \tilde{E} , and s fixed⁶. Clearly, since the initial conditions of Eq.(A.6) were used to find numerically $v(\varphi, \tilde{E}, s)$, this solutions satisfies :

$$v(0, \tilde{E}, 0) = 0 \quad \text{for singlet states} \quad (\text{A.7a})$$

$$v(0, \tilde{E}, 1) = \frac{\pi}{2} \quad \text{for triplet states} \quad (\text{A.7b})$$

Furthermore, the boundary conditions in Eq.(A.6) lead to a transcendental equation valid for singlet and triplet states (which provides a way to find out the eigenvalues) \tilde{E} , and can be written as:

$$v(2\pi, \tilde{E}, s) = -m\pi + v(0, \tilde{E}, s) \quad (\text{A.8})$$

Computationally the problem stated in Eq. (A.8) is analog to find out the zero-roots $\tilde{E}(m, s)$ of the transcendental function $\Xi(\tilde{E}, m, s)$ which has the form:

$$\Xi(\tilde{E}, m, s) = v(2\pi, \tilde{E}, s) + m\pi - v(0, \tilde{E}, s) = 0 \quad (\text{A.9})$$

Thus, the values of \tilde{E} that make $\Xi(\tilde{E}, m, s)$ equal to zero for a given m and s are the eigenenergies $\tilde{E}(m, s) = \tilde{E}_{m,s}$ related to the eigenvalue problem (A.1), and $v_m(\varphi, \tilde{E}_{m,s}, s) = \alpha_{m,s}(\varphi)$ is the phase function related to $\Psi_{m,s}(\varphi)$.

Finally, once obtained the $\alpha_{m,s}(\varphi)$ function and with the aim to compute the amplitude $A(\varphi)$ that allows to rebuild the wavefunction $\Psi_{m,s}(\varphi)$, it is necessary to solve the differential equation easily obtained from relations (A.2):

$$\frac{d}{d\varphi}(A(\varphi)) = A(\varphi)\tan(\alpha(\varphi))[\alpha'(\varphi) + 1] \quad (\text{A.10})$$

Whose direct solution in connection with Eq.(A.1) leads to a numerical integration procedure giving by:

$$A_{m,s}(\varphi) = A_{m,s}(0) \int_0^\varphi \tan(\alpha_{m,s}(\varphi))[1 - \sin^2(\alpha_{m,s}(\varphi)) - \cos^2(\alpha_{m,s}(\varphi))\left(\frac{\tilde{E} - \tilde{V}(\varphi)}{C}\right)] d\varphi \quad (\text{A.11})$$

Where $A_{m,s}(0)$ is a constant factor that can be found by normalizing the system wavefunction.

⁶Note that $v(\varphi, \tilde{E}, s)$ coincides with $\alpha(\varphi)$ function for a \tilde{E} , and s given.

Appendix B

Simplified notation for Low-lying states

A simplified notation defined in Ref.[26, 27] for the some low-lying states related to a two-electron system in one-dimensional rings, has been also used in the present work for labeling the energy states as it is shown in the table B.1. The M , m and s quantum numbers are respectively the center-of-mass and relative angular momenta, and the two-electron spin.

Table B.1: Energy labeling notation for some low-lying states for the two-electron system.

(M, m, s)	<i>Simplified notation</i>
(0, 0, 0)	<i>a</i>
($\pm 1, 1, 1$)	<i>b</i>
(0, 2, 1)	<i>c</i>
($\pm 2, 0, 0$)	<i>d</i>
($\pm 1, 1, 0$)	<i>e</i>
($\pm 2, 2, 1$)	<i>f</i>
(0, 2, 0)	<i>g</i>
($\pm 3, 1, 1$)	<i>h</i>
($\pm 1, 3, 1$)	<i>i</i>
($\pm 3, 1, 0$)	<i>j</i>
($\pm, 2, 2, 0$)	<i>k</i>
(0, 4, 1)	<i>l</i>
($\pm 4, 0, 0$)	<i>m</i>
($\pm 1, 3, 0$)	<i>n</i>
($\pm 3, 3, 1$)	<i>o</i>
($\pm 4, 2, 1$)	<i>p</i>
($\pm 2, 4, 1$)	<i>q</i>

References

- [1] P.M.Petroff, A.Lorke, and A.Imamoglu. *Epitaxially Self-Assembled Quantum Dots. Physics Today*, 2001. [1](#), [2](#), [3](#), [4](#), [38](#)
- [2] H.J.Kimble and S.J.Van Enk. *Push-button teleportation. Nature*, 429:712–713, 2004. [1](#)
- [3] E.L. Wolf. *Nanophysics and Nanotechnology An Introduction to Modern Concepts in Nanoscience*. WILEY-VCH Verlag GmbH & Co, Republic of Germany, 2004. [1](#)
- [4] J. Singh. *Semiconductor optoelectronics Physics and Technology*. McGraw-Hill Series in Electrical and Computing Engineering, 1995. [1](#)
- [5] J.H. Davies. *The Physics of low-dimensional semiconductors an introduction*. Cambridge University Press, USA, 1998. [1](#), [2](#), [4](#)
- [6] J. Singh. *Physics of Semiconductors and Their Heterostructures*. McGraw Hill, Singapore, 1993. [1](#), [26](#)
- [7] L.Esaki and R.Tsu. *Superlattice and negative differential conductivity in semiconductors. J.Res.Dev*, 14:61–65, 1970. [1](#)
- [8] T.Chakraborty. *Quantum Dots*. Elsevier, Amsterdam, 1999. [2](#), [4](#), [8](#)
- [9] Z. M. Wang. *Self-Assembled Quantum Dots*. Springer Science and Business Media,LLC, New York, 2008. [2](#)
- [10] K.Lüdge, M.Bormann, E.Malic, P.Hövel, M.Kuntz, D.Bimberg, A.Knorr, and E.Schöll. *Turn-on dynamics and modulation response in semiconductor quantum dot lasers. Phys.Rev.B*, 78(035316), 2008. [2](#)
- [11] B. Movaghar, S. Tsao, S.Abdollahi Pour, T. Yamanaka, and M. Razeghi. *Gain and recombination dynamics in photodetectors made with quantum nanostructures: The quantum dot in a well and the quantum well. Phys.Rev.B*, 78(115320), 2008. [2](#)

- [12] K.Stewart, M.Buda, J.Wong-Leung, L.Fu, C.Jagadish, A.Stiff-Roberts, and P.Bhattacharya. *Influence of rapid thermal annealing on a stack InAs/GaAs quantum dot infrared photodetector. J.Appl.Phys*, 94:5283–5289, 2003. [2](#)
- [13] I.N.Kaiander, F.Hopfer, T.Kettler, U.W.Pohl, and D.Bimberg. *Alternative precursor growth of quantum dot-based VCSELs and edge emitters for near infrared wavelengths. J.Cryst.Growth*, 272:154–160, 2004. [2](#)
- [14] K.Likharev. *Single Electron Devices and their applications. Proc.IEEE*, 87:606–632, 1999. [2](#)
- [15] J.K.Vincent, V.Narayan, and M.Willander. *Tuning the room temperature nonlinear I-V characteristics of a single-electron silicon quantum dot transistor by split gates: A simple model. Phys.Rev.B*, 65(125309), 2002. [2](#)
- [16] Francisco Javier Culchac, J.C.Granada, and N. Porrás-Montenegro. *Electron ground state in concentric GaAs-(Ga,Al)As single and double quantum ring. phys.stat.sol*, 4:4139–4144, 2007. [3](#)
- [17] R.Rosas, R.Riera, and J.L.Marin. *Electron states in a magnetic quantum ring. J.Phys.Condens.Matter*, 12:6851–6858, 2000. [3](#)
- [18] Hui Hu, Jia-Lin Zhu, and Jia-Jiong Xiong. *Energy levels and far-infrared spectroscopy for two electrons in a nanoscopic semiconductor ring. Phys.Rev.B*, 62:16777–16783, 2000. [3](#)
- [19] A.Puente and L.Serra. *Ground state and far-infrared absorption of two-electron rings in a magnetic field. Phys.Rev.B*, 63, 2001. [3](#)
- [20] Hui Hu, J.-L. Z., Dai-Jun Li, and Jia-Jiong Xiong. *Aharonov-Bohm effect of excitons in nanorings. Phys.Rev.B*, 63:16777–16783, 2001. [3](#)
- [21] J.Song and S.E. Ulloa. *Magnetic field effects on quantum ring excitons. Phys.Rev.B*, 63:16777–16783, 2001. [3](#)
- [22] R.A. Römer and M.E. Raikh. *Para and Ortho-Trions on a Ring: A Simple Mode. phys.stat.sol*, 227:381–385, 2001. [3](#)
- [23] C.M. Lee and J.K.F. Yau. *Impurity effect on low-lying spectra in an electron magnetic dot. Physics Letters A*, 300:140–146, 2002. [3](#), [20](#)
- [24] H.Pan and J.-L.Zhu. *Impurity effects on energy levels and far-infrared spectra of nanorings. Journal of Physics and Condensed Matter*, 15:7287–7295, 2003. [3](#), [20](#)

- [25] Axel Lorke, R.J.Luyken, Alexander O. Govorov, and Jörg P. Kotthaus. *Spectroscopy of Nanoscopic Semiconductor Rings*. *Phys.Rev.let*, 84:2223, 2000. [3](#), [4](#), [22](#), [41](#), [49](#)
- [26] J.-L.Zhu and Z. Dai. *Two electrons in one-dimensional nanorings: Exact solutions and interaction energies*. *Phys.Rev.B*, 68, 2003. [3](#), [6](#), [22](#), [23](#), [24](#), [31](#), [32](#), [33](#), [34](#), [41](#), [43](#), [49](#), [52](#), [63](#)
- [27] Jairo H. Marin, Francisco García, and Ilia D. Mikhailov. *Two Electrons in Vertically Coupled One-Dimensional Rings*. *Braz.J.Phys*, 36, 2006. [3](#), [5](#), [6](#), [21](#), [23](#), [31](#), [32](#), [41](#), [43](#), [49](#), [52](#), [63](#)
- [28] J.C. Ahn, H.Y. Kang, , and O'Dae Kwon. *Angle-dependent multiple-wavelength radial emissions in a toroidal microcavity : (A photonic quantum ring laser)*. *SPIE*, 3283:241–251, 1998. [3](#)
- [29] Dai Jong-Horng, Lin Yi-lung, and Lee Si-Chen. *Voltage-Tunable Dual-Band In(Ga)As Quantum-Ring Infrared Photodetector*. *IEEE Photonics Technology Letters*, 19, 2007. [3](#)
- [30] Ferran Suárez et al. *Laser devices with stacked layers of InGaAs/GaAs quantum rings*. *Nanotechnology*, 15:S126–S130, 2004. [3](#)
- [31] A. Bruno-Alfonso and A. L. *Semiconductor quantum rings: Shallow-donor levels*. *Phys.Rev.B*, 61, 2000. [3](#)
- [32] Guang-Yin Chen, Yueh-Nan Chen, and Der-San Chuu. *The Aharanov-Bohm effect in concentric quantum double rings*. *Solid State Communications*, 143, 2007. [3](#), [5](#), [41](#)
- [33] N Levine. *Química Cuántica*. Prentice Hall, New York, 2001. [3](#), [4](#)
- [34] C.A.Gómez, L.F García, W. Gutiérrez, and J.H.Marín. *Ion-molecular D2+ complex in a quantum ring*. *Microelectronic Journals*, 39:1279, 2008. [3](#), [5](#), [20](#), [21](#), [41](#), [42](#)
- [35] Ralf Blossey and Axel Lorke. *Wetting droplet instability and quantum ring formation*. *Phys.Rev.E*, 65:021603, 2002. [4](#)
- [36] J.J Sakurai. *Modern Quantum Mechanics*. Addison-Wesley, USA, 1994. [4](#)
- [37] D.J Griffiths. *Introduction to Quantum Mechanics*. Prentice Hall, New Jersey, 1995. [4](#), [8](#), [14](#), [45](#), [61](#)
- [38] W Greiner. *Quantum Mechanics: an Introduction*. Springer, Berlin, 2000. [4](#), [15](#), [16](#), [45](#), [61](#)

- [39] R.G. Parr and W Yang. *Density-Functional Theory of Atoms and Molecules*. Oxford University Press, New York, 1989. 4
- [40] Umrigar Cyrus J. Nightingale, M.P. *Quantum Montecarlo Methods in Physics and Chemistry*. Springer, London, 1999. 4
- [41] S. Sanguinetti, M.Abbarchi, A.Vinattieri, M.Zamfirescu, M.Gurioli, T.Mano, T.Kuroda, and N.Koguchi. *Carrier dynamics in individual concentric quantum rings: Photoluminescence measurements*. *Phys.Rev.B*, 77, 2008. 4, 5, 31, 32
- [42] Dirk Kahler, U. K.and Dirk Reuter, and Andreas D. Wieck. *Aharonov-Bohm effect in nanoscale quantum rings fabricated from compensating-layer GaAs/AlGaAs heterostructures*. *Physica E*, 17:284–285, 2003. 4
- [43] Z.R. Wasilewski and S.F.and J.P. McCalrey. *Size and shape engineering of vertically stacked self-assembled quantum dots*. *Journal of Crystal Growth*, 201/202:1131–1135, 1999. 5
- [44] J.I. Climente, J.P.and M. Barranco, F. Malet, and M. Pi. *Electronic structure of few-electron concentric double quantum rings*. *Phys.Rev.B*, 73, 2006. 5
- [45] F. Malet, M.Barranco, E. Lipparini, R. Mayol, and M. Pi. *Vertically coupled double quantum rings at zero magnetic field*. *Phys.Rev.B*, 73, 2006. 5
- [46] B. Szafran and S. B.and M. Dudziak. *Electron correlations in charge coupled vertically stacked quantum rings*. *Phys.Rev.B*, 75, 2007. 5
- [47] Steven E. Koonin and Dawn C.Meredith. *Computational Physics, Fortran version*. Westview Press, USA, 1990. 9, 10, 59
- [48] Claude Cohen-Tannoudji, Bernard Diu, and Franck Laloe. *Quantum Mechanics*. John Wiley and Sons, Paris, 1977. 14, 45
- [49] Christopher J. Cramer. *Essentials of Computational Chemistry, Theories and Models*. Wiley, England, 2004. 14
- [50] Tao Pang. *An Introduction To Computational Physics*. Cambridge University Press, New York, 2006. 21, 59
- [51] William.H Press, Saul A. Teukolsky, William.T Vetterling, and Brian.P Flannery. *Numerical Recipes in FORTRAN 77: The Art of Scientific Computing*. Cambridge University Press, New York, 1992. 21, 59

- [52] F.J.Betancur, I.D.Mikahailov, and L.E.Oliveira. *Shallow donor states in GaAs-(Ga, Al)As quantum dots with different potential shapes. J.Appl.Phys.D*, 31:3391, 1998. [21](#), [22](#)
- [53] D.Granados, J.M.García, T.Ben, and S.I. Molina. *Vertical order in stacked layers of self-assembled In(Ga)As quantum rings on GaAs (001). Appl.Phys.Lett*, 86:071918, 2005. [22](#)
- [54] T.Ihn, A. Fuhrer, T.Heinzel, K.Ensslin, W.Wegscheider, and M.Bichler. *Marvellous things in marvellous rings: energy spectrum, spins and persistent currents. Physica E*, 16:83, 2003. [22](#)
- [55] F. Bolton. *Monte-Carlo calculation of few-electron systems in quantum dots . Solid State Electron*, 37:1159, 1994. [22](#)
- [56] A. Matulis and F. M. Peeters. *Renormalized perturbation series for quantum dots . J.Phys.Condens.Matter*, 6:7751, 1994. [22](#)
- [57] M.Susuki, D.Tsuya, S.Moriyoma, T.Fuse, and K.Shisbashi. *Carbon nanotubes as a building block of quantum dot devices. Physica E*, 24:10, 2004. [30](#)
- [58] V.Ya Prinz. *Precise semiconductor nanotubes and nanoshells fabricated on (1 1 0) and (1 1 1) Si and GaAs. Physica E*, 23:260, 2004. [30](#)
- [59] V.Ya Prinz. *Precise semiconductor nanotubes and nanocorrugated quantum systems. Physica E*, 24:54, 2004. [30](#)
- [60] A.B.Vorobev, V.Ya Prinz, Yu.S.Yukecheva, and A.I.Toropov. *Magnetotransport properties of two-dimensional electron gas on cylindrical surface. Physica E*, 23:171, 2004. [30](#)
- [61] G.Ferrari, A.Bertoni, G.Goldoni, and E.Molinari. *Cylindrical two-dimensional electron gas in a transverse magnetic field. Phys.Rev.B.*, 78:115326, 2008. [30](#)
- [62] Lucjan Jacak, Pawel Hawrylak, and Arkadiusz Wojs. *Quantum Dots*. Springer, Berlin, 1997. [31](#), [32](#)
- [63] L.F.García, I.D.Mikhailov, and J.H.Marín. *Spectrum of two spatially separated particles in coaxial nanoring. Rev.Col.de Fís.*, 38:1078, 2006. [32](#), [35](#)
- [64] T.Mano, T.Kuroda, S.Sanguinetti, T.Ochiai, T.Tateno, J.Kim, T.Noda, M.Kawabe, K.Sakoda, G.Kido, and N.Koguchi. *Self-Assembly of Concentric Quantum Double Rings. Nano Lett.*, 5:425–428, 2005. [41](#)

- [65] M.Bayer, P.Hawrylak, K.Hinzer, S.Fafard, M.Korkusinski, Z.R.Wasilewski, O.Stern, and A.Forchel. *Coupling and Entangling of Quantum States in Quantum Dot Molecules. Science*, 291:451–453, 2001. [41](#)
- [66] Viefers, P. Koskinen, D.P.Singha, and M.Manninen. *Quantum rings for beginners: Energy spectra and persistent currents. Physica E*, 21:1, 2004. [41](#)
- [67] H-T.Li, L-Z.Liu, and J-J.Liu. *Electronic States of Elliptical Quantum Rings Subjected to a Magnetic Field. Chin.Phys.Lett.*, 25:4101, 2008. [41](#)
- [68] M.Encinosa. *Electron wave functions on T2 in a static magnetic field of arbitrary direction. Physica E*, 28:209–218, 2005. [41](#)
- [69] F.García, J.H.Marín, H.Paredes, and I.D.Mikhailov. *Low lying states of two electron quasi-one-dimensional ring. Phys.Stat.Sol.(c)*, 2:3630–3633, 2005. [41](#)
- [70] J.Betancur, W.Gutiérrez, and J.Pina. *Energy spectrum of on-axis negatively charged donor in toroidal-shaped ring . Physica B*, 396:12–15, 2007. [49](#)
- [71] W.Kolos and L.Wolniewicz. *Potential-Energy Curves for the $X^1, \Sigma_g^+, b^3\Sigma_u^+$, and $C^1\Pi_u$ States of the Hydrogen Molecule. J.Chem.Phys.*, 43:2429, 1965. [52](#)
- [72] Y.Aharonov and D.Bohm. *Significance of Electromagnetic Potentials in the Quantum Theory. Phys.Rev.*, 115:485–491, 1959. [56](#)
- [73] Paul Harrison. *Quantum Wells, Wires and Dots*. Wiley, United Kingdom, 2005. [57](#)